Title

Strength of CAR signaling determines T cell versus ILC differentiation from pluripotent stem cells

Journal

Cell Reports, 42(3)

ISSN

2639-1856

Authors

Li, Suwen

Wang, Chloe S

Montel-Hagen, Amélie

et al.

Publication Date

2023-03-01

DOI

10.1016/j.celrep.2023.112241

Peer reviewed

HHS Public Access

Author manuscript

Cell Rep. Author manuscript; available in PMC 2023 July 02.

Published in final edited form as:

Cell Rep. 2023 March 28; 42(3): 112241. doi:10.1016/j.celrep.2023.112241.

Strength of CAR signaling determines T cell versus ILC differentiation from pluripotent stem cells

Suwen Li[1,2,3], **Chloe S. Wang**[1], **Amélie Montel-Hagen**[2,8], **Ho-Chung Chen**[2], **Shawn Lopez**[2], **Olivia Zhou**[1], **Kristy Dai**[1], **Steven Tsai**[1], **William Satyadi**[1], **Carlos Botero**[1], **Claudia Wong**[1], **David Casero**[2,9], **Gay M. Crooks**[2,4,5,6,7,10], **Christopher S. Seet**[1,5,6,7,10,11,*]

[1]Department of Medicine, Division of Hematology-Oncology, David Geffen School of Medicine (DGSOM), University of California, Los Angeles, Los Angeles, CA 90095, USA

[2]Department of Pathology and Laboratory Medicine, David Geffen School of Medicine, University of California, Los Angeles, Los Angeles, CA 90095, USA

[3]Department of Molecular and Medical Pharmacology, David Geffen School of Medicine, University of California, Los Angeles, Los Angeles, CA 90095, USA

[4]Department of Pediatrics, David Geffen School of Medicine, University of California, Los Angeles, Los Angeles, CA 90095, USA

[5]Broad Stem Cell Research Center (BSCRC), David Geffen School of Medicine, University of California, Los Angeles, Los Angeles, CA 90095, USA

[6]Jonsson Comprehensive Cancer Center (JCCC), David Geffen School of Medicine, University of California, Los Angeles, Los Angeles, CA 90095, USA

[7]Molecular Biology Institute, University of California, Los Angeles, Los Angeles, CA 90095, USA

[8]Present address: Pluto Immunotherapeutics, Los Angeles, CA, USA

[9]Present address: F. Widjaja Inflammatory Bowel Disease Institute, Cedars Sinai Medical Center, 8700 Beverly Blvd., Los Angeles, CA 90048, USA

[10]Senior author

[11]Lead contact

SUMMARY

[*]Correspondence: cseet@mednet.ucla.edu.

AUTHOR CONTRIBUTIONS

Conceptualization, S. Li, G.M.C., and C.S.S.; methodology, S. Li, A.M.-H., and C.S.S.; formal analysis, S. Li, C.S.W., D.C., and C.S.S.; investigation, S. Li, C.S.W., A.M.-H., H.-C.C., S. Lopez, O.Z., W.S., C.B., S.T., C.W., and C.S.S.; writing – original draft, S. Li and C.S.S.; writing – review & editing, S. Li, G.M.C., and C.S.S.; Supervision, G.M.C. and C.S.S.; funding acquisition, G.M.C. and C.S.S.

DECLARATION OF INTERESTS

A.M.-H., G.M.C., and C.S.S. are co-founders and scientific consultants to Pluto Immunotherapeutics, which holds certain rights relating to the ATO system. A.M.-H. is a current employee of Pluto Immunotherapeutics.

SUPPLEMENTAL INFORMATION

Supplemental information can be found online at https://doi.org/10.1016/j.celrep.2023.112241.

Generation of chimeric antigen receptor (CAR) T cells from pluripotent stem cells (PSCs) will enable advances in cancer immunotherapy. Understanding how CARs affect T cell differentiation from PSCs is important for this effort. The recently described artificial thymic organoid (ATO) system supports *in vitro* differentiation of PSCs to T cells. Unexpectedly, PSCs transduced with a CD19-targeted CAR resulted in diversion of T cell differentiation to the innate lymphoid cell 2 (ILC2) lineage in ATOs. T cells and ILC2s are closely related lymphoid lineages with shared developmental and transcriptional programs. Mechanistically, we show that antigen-independent CAR signaling during lymphoid development enriched for ILC2-primed precursors at the expense of T cell precursors. We applied this understanding to modulate CAR signaling strength through expression level, structure, and presentation of cognate antigen to demonstrate that the T cell-versus-ILC lineage decision can be rationally controlled in either direction, providing a framework for achieving CAR-T cell development from PSCs.

In brief

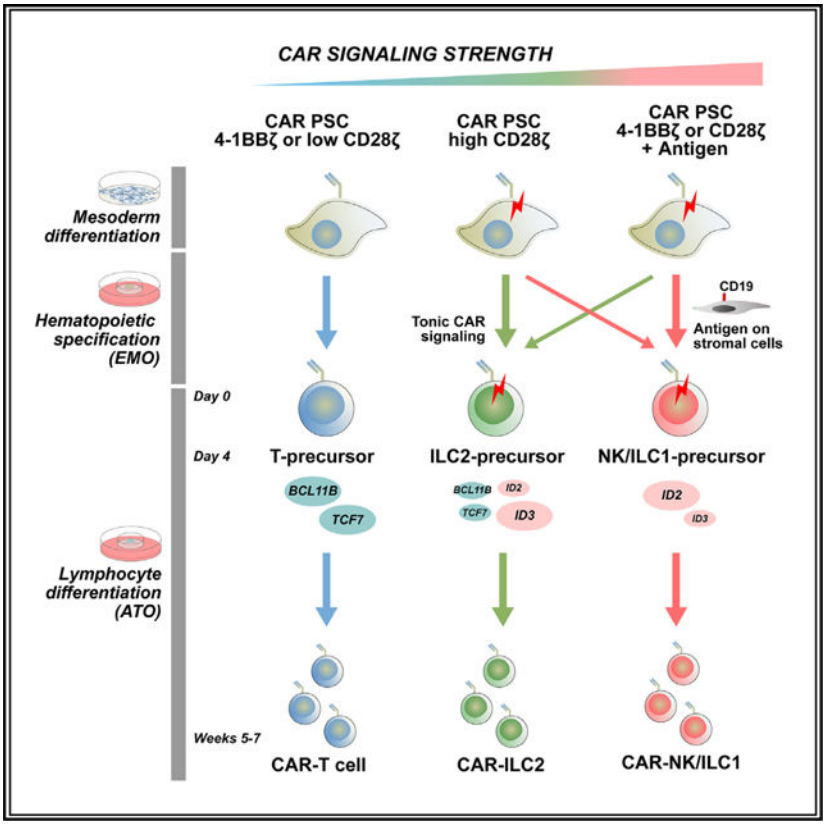

Li et al. show that tonic CAR activation during early lymphoid development from pluripotent stem cells (PSCs) diverts T cell development to innate lymphoid cell lineages. They show that tuning CAR tonic signaling via alternative costimulatory domains enables preservation of conventional CAR-T cell differentiation from PSCs.

INTRODUCTION

Autologous chimeric antigen receptor (CAR)-T cells have shown great promise for treatment of advanced malignancies. *In vitro* generation of allogeneic CAR-T cells from CAR-engineered "master" pluripotent stem cell (PSC) lines has the potential to expand patient access to CAR-T cell therapies.[1,2] In contrast to peripheral blood T cells, however, constitutive expression of CARs in PSCs or primary hematopoietic stem/progenitor cells (HSPCs) may perturb critical early stages of T cell differentiation because of tonic or antigen-induced CAR signaling during lymphoid development, and indeed the first demonstration of T cell differentiation from CAR-transduced PSCs reported cells with an innate phenotype and function reminiscent of γδ T cells.[3] Complicating this picture is a wide range of signaling strengths achievable through modifications to CAR expression level and structural or signaling elements,[4–8] rendering studies of the impact of CARs on T cell differentiation specific to each CAR and expression system used.

We recently developed the artificial thymic organoid (ATO) system, a 3D culture method that supports mature effector T cell differentiation from PSCs and human HSPCs *in vitro*.[9,10] We used this platform to systematically interrogate the effect of constitutive lentiviral expression of different CD19-targeted CARs on lymphoid development from PSCs. We report the unexpected finding that certain CD28ζ-based CD19 CARs divert T lineage commitment to the closely related innate lymphoid cell 2 (ILC2) lineage, resulting in a nearly complete loss of CAR-T cell output but generation of functionally mature CAR-ILC2s.

ILC2s are a helper-type ILC lineage characterized by a predominantly type 2 cytokine response to epithelium-derived alarmins, including interleukin-25 (IL-25), IL-33, and thymic stromal lymphopoietin (TSLP).[11,12] Despite not being subject to recombination activating gene (RAG)-mediated T cell receptor (TCR) rearrangement during development, ILC2s share many developmental similarities with T cells, including a requirement for Notch and IL-7 receptor signaling and potential intrathymic differentiation from common T/ILC2-primed lymphoid progenitors.[13–15] Despite these similarities, specific determinants of T versus ILC2 lineage bifurcation from lymphoid progenitors remain poorly understood. In contrast, transcriptional regulation of ILC2 development has been characterized in detail in mice, sharing key transcription factors with developing T cells, including BCL11B, TCF7, and GATA3,[16–22] superimposed on which is ID2-mediated inhibition of E-protein activity essential for suppressing T cell lineage potential, a mechanism common to ILC2 and natural killer (NK)/ILC1 lineage commitment.[23–26]

We used the unexpected finding of CAR-mediated T-to-ILC2 lineage diversion in ATOs to elucidate the timing and potential mechanisms of CAR-mediated ILC2 differentiation in this system and identified strategies for mitigating the CAR-imposed block in T differentiation or, conversely, directing ILC commitment from PSCs. We present these findings as a starting point for modeling human T/ILC differentiation and as a framework for understanding the effects of CARs on the development of conventional CAR-T cells and other lymphoid lineages from PSCs.

RESULTS

CAR-induced ILC2-biased lymphoid differentiation from PSCs

We applied the ATO differentiation system to study the effect of CAR expression during T cell development from human PSCs. Using a lentiviral vector system previously validated for TCR expression in PSC ATOs,[9] we transduced the H1 embryonic stem cell (ESC) line[27] with a second-generation CD19-targeted CAR containing an FMC63 single-chain variable fragment (scFv), immunoglobulin G4 (IgG4) CH2/CH3 long spacer and hinge, and CD28 transmembrane (TM), CD28 costimulatory, and CD3ζ signaling domains[28–30] (Figure S1A) 2A-linked to EGFP to generate a stable, clonal, CAR-expressing PSC line (H1-CAR). Surface CAR expression on H1-CAR PSCs was readily detected using an anti-FMC63 antibody (Figure S1B). Lymphocyte differentiation followed a three-phase protocol as described previously,[9] comprising feeder-free generation of embryonic-like mesoderm progenitors (EMP) followed by aggregation with the MS5-human Delta-like ligand 4 (MS5-hDLL4) stromal cell line in 3D, air-fluid interface culture on permeable cell culture inserts to form embryonic mesoderm organoids (EMOs), which supported mesoderm (day −14 to day −7) and hematopoietic (day −7 to day 0) specification. In a modification of the original protocol, non-adherent cells were isolated from EMOs on day 0 and reaggregated at a defined ratio with fresh MS5-hDLL4 cells to form ATOs, which supported T cell commitment and maturation (day 0 to weeks 5–7) (Figure 1A).

Analysis of H1 PSC ATOs showed orderly T cell differentiation from T-lineage (CD7+CD5+), CD4−CD8− double-negative (DN) precursors to CD4+CD8+ double-positive (DP) precursors, CD3+TCRαβ+ “late” DP precursors and, ultimately, CD3+TCRαβ+CD8+CD4−single-positive (CD8SP) mature T cells between weeks 3 and 6 (Figure 1B). As reported previously, at week 6, CD3+TCRαβ+CD4+CD8− SP (CD4SP) T cells were a clear but minor population, as were CD3+TCRαβ− cells (shown previously to be enriched for TCRγδ T cells).[9] In contrast, H1-CAR ATOs, while still producing CD7+ lymphoid cells, exhibited a block in T cell lineage differentiation, generating a transient population of DP precursors at week 3 but largely failing to develop CD3+TCRαβ+ T cells at week 6 (Figure 1B). TCRγδ cells developed at low levels under both ATO conditions (Figure S1C). Despite impaired T cell generation in H1-CAR ATOs, cell numbers at week 6 were preserved (Figure 1C) and comprised predominantly CD7+ lymphoid cells (Figure 1B), prompting us to look for evidence of ILC generation.

For flow cytometry analysis of week 6 ATOs, we defined T-lineage cells as CD4+ (including immature CD4 SP and early DP precursors) and/or CD3+ (including late DP and SP T cells) (Figure S1D). Because the remaining CD3−CD4− population could also theoretically contain DN T cell precursors, we sorted this population from H1 or H1-CAR ATOs at week 2 and compared their T cell potential with T-lineage committed DP precursors by reaggregation in new ATOs. While DP precursors differentiated to CD3+ CD8SP T cells as expected, CD3−CD4− cells did not give rise to DP precursors or CD3+ T cells, instead producing mainly CD56+ cells, suggesting clearance of T cell precursors within the CD3−CD4− population by week 2 (Figure S1F). Further analysis of the CD3−CD4− population in H1-CAR ATOs at week 6 showed a subset of CD7+ cells with heterogeneous

expression of CD2, CD5, CD56, and CD8α (Figure S1E), accounting for less than 10% of CD45+ cells (Figure 1E). Based on these minimal surface markers, we designated this population "NK/ILC1 enriched" because of difficulty in distinguishing between human group 1 ILC populations based on surface markers.[31–34] While a small, CD117+ population was detected, CD117+ NKp44+ ILC3s were not seen (Figure 1E). Surprisingly, however, a majority of cells, including the CD117+ subset, showed an ILC2 phenotype defined as CD7+CD200R+CD25^{hi} (Figure S1D). Using these lineage definitions, we tracked lymphoid development in H1 or H1-CAR ATOs over 6 weeks and saw a striking emergence of the ILC2-like population over time in H1-CAR but not H1 ATOs (Figure 1F). We determined that this CAR-mediated T cell-to-ILC2 diversion was not specific to the H1 ESC line because a second line, ESI-017,[35] revealed the same ILC2 bias in ATOs when transduced with the same CAR construct (Figure S1G).

Further examination of the ILC2-like population revealed co-expression of canonical ILC2 surface markers, including CRTH2, CD161, and ICOS,[36] and negativity for T or NK markers, including CD2, CD27, and CD56 (Figure 2A). High expression of CD200R and CD25 was therefore used to identify this ILC2-like population in subsequent analyses. The ILC2 identity of these cells was further confirmed by intracellular staining, which showed high expression of GATA3 and low levels of Eomes, T-bet, and RORγt (Figure 2B). To further characterize these cells, we performed RNA sequencing (RNA-seq) on sorted DN cells from H1-CAR ATOs compared with CD8SP T cells from standard, week 6 H1 ATOs. This revealed, in the H1-CAR DN population, an ILC2 gene signature that included expression of the ILC2-defining cytokine receptors *IL1RL1* (IL33R/ST2) and *IL17RB* (IL25R); type 2 cytokines, including *CSF2* (GM-CSF), *IL4*, and *IL13*; and the T cell/ILC2-associated transcription factors *GATA3* and *TCF7* (Figures 2C and S2). Expression of cytotoxic granule-associated genes, including *GZMB*, *GZMA*, *GZMH*, and *PRF1*, was low, consistent with a helper ILC phenotype (Figure S2). Interestingly, while the canonical ILC transcription factor *ID2* was expressed at similar levels between H1-CAR DN (ILC2-like) and CD8SP T cells, expression of its functional homolog, *ID3*, was specific to the ILC2-like population (Figure S2). Gene set enrichment analysis[37] of gene signatures from primary human fetal ILC2s and T cells[38] showed that H1-CAR DN gene expression correlated positively with the ILC2 gene signature and negatively with the T cell signature, whereas the opposite was true for H1 ATO-derived CD8SP T cells (Figure 2D). We also looked within the H1-CAR DN transcriptome for the presence of tissue-specific ILC2 gene signatures based on human blood, lung, and tonsil ILC2 profiles,[39] but no differential enrichment was observed (data not shown), reflecting either absent tissue subspecialization of *in vitro*-derived ILC2s and/or population heterogeneity not resolvable by bulk RNA-seq.

CAR-ILC2 are type 2 cells subject to functional plasticity

We next confirmed that H1-CAR ILC2-like cells were functional ILC2s. Freshly isolated CAR-ILC2s from ATOs robustly produced the type 2 cytokines IL-4, IL-13, and GM-CSF in response to phorbol 12-myristate 13-acetate (PMA)/ionomycin as well as IL-2 and tumor necrosis factor alpha (TNF-α) (Figure 2E), which have been shown to be produced by ILC2s in mice and humans.[40,41] While primary ILC2s lack antigen-specific receptors, CAR-ILC2s surprisingly expanded in response to CD19+ NALM6 cells in the presence of IL-7 and

IL-2, which was modestly increased by addition of IL-25, IL-33, and TSLP (Figure 2F), indicating intact functionality through the CAR.

Several studies have also described helper plasticity of ILC2s in response to IL-12, resulting in type 1 "polarized" ILC2s capable of producing interferon γ (IFNγ).[42–45] We tested the type 1 plasticity potential of CAR-ILC2s by culturing them with IL-7 and IL-2 in combination with IL-25, IL-33, and TSLP or IL-12, followed by PMA/ionomycin stimulation. Culture with IL-25/IL-33/TSLP resulted in induction of the type 2 cytokine IL-5, not seen in unstimulated CAR-ILC2s (Figure 2E) and possibly reflecting maturation to an IL-5-producting state by one or more of these "ILC2" cytokines. While some IFNγ production was seen under this condition, culture with IL-12 greatly increased the frequency of IFNγ-producing cells and suppressed emergence of IL-5-producing cells, consistent with the type 1 plasticity seen in primary ILC2s (Figures 2G and 2H).

CAR activation in early lymphoid precursors precedes ILC2-biased differentiation

We next sought to understand the CAR-mediated transcriptional changes leading to ILC2 differentiation in H1-CAR ATOs. We first analyzed global hematopoietic differentiation in H1 and H1-CAR ATOs by flow cytometry and single cell RNA-seq (scRNA-seq) at the ATO day 0, day 4, and day 7 time points. Flow cytometry at these early time points showed no obvious differences in hematopoietic differentiation based on expression of CD43 and CD45 (Figure 3A), but an increase in lymphoid-to-erythroid ratio was seen in H1 relative to H1-CAR ATOs on day 7 based on CD7 and CD235a expression (Figure 3B). scRNA-seq at these time points revealed multilineage hematopoietic differentiation based on lineage-defining genes (Figures 3C–3E; Table S1). Across all samples, gene expression clusters were annotated as megakaryocyte (exemplified by expression of *PPBP*, *PF4*, and *GP1BB*), erythroid (*HBZ, HBA1*, *HBG1*, *GYPA*, and *KLF1*), myeloid, and lymphoid lineages. Myeloid clusters comprised monocyte (*FCER1G*, *CTSD*, *CD68*, and *CTSS*), neutrophil (*DEFA3*, *MPO*, and *AZU1*), and eosinophil (*EPX*, *PRG3*, and *IL5RA*) clusters as well as a surprisingly prominent mast cell cluster (*GATA2*, *CPA3*, and *HPGD*) (Figures 3C–3E). The lymphoid cluster expressed *IL7R*, *CD7*, *CD3D*, *CD3G*, and *CD247*, with a B cell signature notably absent. Also absent was a clear signature of HSPCs, suggesting that multipotent progenitor cells may have emerged and differentiated within the preceding EMO stage, prior to ATO day 0. Aside from a slightly higher lymphoid-to-erythroid cluster ratio in H1 ATOs on day 7 (Figures 3F, 3G, and S3), no major CAR-associated differences in multilineage cluster dynamics were appreciated (Figures 3F, 3G, and S3).

Because a multipotent progenitor stage was not identified, we focused our attention on the lymphoid-specified cluster characterized by expression of *IL7R* and *CD7*. To validate that our analysis represented early lymphoid progenitors/precursors rather than mature lymphocytes, we determined by flow cytometry that mature ILC2s (co-expressing CD200R and CD25) were rare, representing no more than 0.8% of ATOs on day7 (Figure S4A). Within the CD7+ population, immature SP CD4+ (ISP4) and some CD3-negative early DP T cell precursors were seen on day 7, with the frequency of DP precursors markedly lower in H1-CAR compared with H1 ATOs, suggesting an already evident block in T cell differentiation in H1-CAR ATOs (Figure S4B).

By scRNA-seq, reclustering of the lymphoid cluster revealed multilymphoid development (Figures 4A, 4B, S4C, and S4D). Globally, there was expression of *IL7R* and, surprisingly, the TCR components *CD3D*, *CD3E*, *CD3G*, and *CD247* across all lymphoid clusters (Figures 4C and S4F). A major contingent contained precursors identified as T cell, ILC2, or NK/ILC1 lineage based on canonical genes (Figure 4A). The T cell lineage precursor cluster was defined by expression of *RAG1*, *PTCRA*, and *CD8B*, whereas the ILC2 precursor cluster was negative for these but expressed *GATA3*, *PTGDR2*, and *IL1RL1* (Figures 4B and 4C; Table S2). NK/ILC1 precursors expressed *GNLY*, *GZMB, KLRC1, TBX21*, and high *ID2* (Figures 4B and 4C; Table S2). While NK/ILC1 precursors were seen at a similar frequency in H1 and H1-CAR ATOs, the ILC2 and T lineage clusters showed an inverse relationship between the H1 and H1-CAR ATOs (Figures 4D, 4E, S4C, and S4D). Outside of these three main clusters, a small ILC3-lineage cluster expressed high levels of *ID2*, *RORC*, and *KIT* (Figures 4B and 4C; Table S2). *CD52*, reported to be highly expressed on human ILC-primed bone marrow progenitors,[46] was higher in all ILC-lineage clusters relative to the T cell-lineage cluster (Figure 4C; Table S2). An unexpected *KLF1*+ and *GYPA*+ erythroid-like cluster that co-expressed low levels of *IL7R*, *CD7*, and CD3 genes was of unclear significance (Figures 4B and 4C). Finally, a small cluster containing cells expressing *IL7R*, *CD7*, *CD3D*, and *CD34* was the sole lymphoid cluster on day 0 and was not detected by day 4 (Figures 4B, 4C, S4C, and S4D). This cluster also expressed within it the embryonic hematopoietic progenitor-associated genes *SPI1*, *SPINK2*, and *RUNX1* (Figure 4C), but a larger proportion expressed myeloid genes, including *MPO*, *LYZ*, and *AZU1* (Table S2), making the ultimate relationship of this putative progenitor cluster to later lymphoid lineage clusters unclear.

Focusing on transcription factors expressed within the T cell, ILC2, and NK/ILC1 precursor clusters, all three were noted to share expression of *RUNX3* and *ETS1* (Figure 4F). The NK/ILC1 cluster showed high levels of *TBX21* and *ID2*. The T cell and ILC2 clusters shared expression of *TCF7* and *BCL11B*, whereas high *GATA3* and *ID3* expression distinguished ILC2 from T cell lineage clusters (Figures 4F and 4G). Canonical NK/ILC1 lineage genes, including *ZBTB16* (encoding PLZF), *ZNF683* (encoding HOBIT), *GNLY*, *NKG7*, and *FCER1G*, were also seen in the ILC2 cluster, but at much lower levels than in the NK/ILC1 cluster (Figures 4C and 4F; Table S2). *ID2* has been shown to enforce NK and ILC2 lineage commitment in mice through suppression of E-protein activity.[24,25,47] Consistent with this, *ID2* was expressed in NK/ILC1 and ILC2 clusters (Figure 4G). Induction of *ID2* and *ID3* was first evident in H1-CAR ATOs at the day 4 time point, coinciding with emergence of the dominant ILC2 and NK/ILC1 clusters, compared with day 7 in H1 ATOs, suggesting premature induction of these T cell lineage-inhibitory transcription factors in H1-CAR lymphoid precursors (Figure S4E). Surprisingly, *ID2* expression was lower in the ILC2 than NK/ILC1 cluster, and instead its functional homolog, *ID3*, was highly expressed (Figures 4F and 4G). Indeed, *ID3* expression had been observed to be high in mature CAR-ILC2s (Figures 2C and S2), a finding also reported for human neonatal ILC2s.[48]

Having identified putative ILC2 precursors enriched in early H1-CAR ATOs, we performed pathway analysis on genes differentially expressed between the ILC2 and T cell precursor clusters. ILC2 precursors showed relatively less enrichment of Notch, Wnt, and aryl hydrocarbon receptor pathways relative to T cell precursors (Figure S4G). However, in

the ILC2 cluster, we saw unexpected enrichment of genes associated with TCR signaling and T cell activation (Figure 4H). Gene sets associated with STAT3 and cytokine receptor signaling were also enriched, as were actin cytoskeleton remodeling pathways, the latter possibly suggesting CAR-derived CD28 signaling, which has been shown to mediate TCR-independent cytoskeletal remodeling in T cells.[49] Overall, we reasoned that the signature of TCR activation in ILC2 precursors represented constitutive CAR activation. Indeed, the critical CD3ζ signal transduction molecules *LCK*, *ZAP70*, and *LAT* were expressed in all lymphoid clusters, supporting potential for CAR activation even at these very early lymphoid precursor stages (Figure 4I). Enrichment of the TCR activation gene *CD69* within the ILC2-lineage cluster provided further indirect support of CAR activation in ILC2 precursors (Figure 4I).

Tuning CAR signaling strength permits rational control of CAR-T cell versus ILC development

Because constitutive CAR signaling was likely driving T cell-to-ILC2 lineage diversion in ATOs, we reasoned that modulating CAR signaling strength may offer specific control over T cell versus ILC2 output. First, to exclude the possibility of antigen-dependent CAR signaling in ATOs, we confirmed that CD19 expression was not detected by scRNA-seq, consistent with the absence of a B-lineage cluster. We therefore tested approaches to modulate antigen-independent “tonic” CAR signaling in ATOs.

Previous reports have shown that the CAR expression level affects signaling strength and, thus, functional outcomes in mature CAR-T cells.[50,51] We therefore tested the effect of varying CAR expression level on T cell versus ILC2 output in ATOs. Using the CD19-targeted CD28ζ CAR vector used in previous experiments, we derived two additional H1-CAR lines with progressively lower CAR expression levels (designated H1-CAR-med and H1-CAR-low, respectively, with the original H1-CAR line designated H1-CAR-high in these experiments) (Figure 5A). Interestingly, surface CAR expression only loosely correlated with vector copy number in these PSC lines (Figures 5A and S5A). Upon differentiation in ATOs, we observed a dose-dependent positive correlation between CAR expression level and ILC2 output, with H1-CAR-high ATOs showing strong ILC2 output and a nearly complete block in T cell differentiation, while H1-CAR-low ATOs showed little ILC2 generation and preservation of normal T cell differentiation, including maturation to CD3+TCRαβ+ CD8SP CAR-T cells (Figures 5B and 5C). H1-CAR-med ATOs showed an intermediate, ILC2-biased lineage output. CAR-ILC2 cells derived from these PSC lines retained their respective levels of surface CAR expression (Figure 5D). We next tested whether phenotypically normal CD8SP CAR-T cells generated in H1-CAR-med and H1-CAR-low ATOs were functional through the CAR. While the small number of CD3+ CAR-T cells generated in H1-CAR-med ATOs showed CD19-dependent activation, as seen by downregulation of surface CAR[50,52] and upregulation of CD25 in response to CD19+ but not CD19-knockout Raji cells, T cells from H1-CAR-low ATOs showed defective antigen-dependent activation (Figure 5E), indicating that the CAR expression level below which normal T cell differentiation occurred was also suboptimal for antigen-dependent effector CAR-T cell function.

We took advantage of weak CAR signaling in the H1-CAR-low PSC line to prospectively test the hypothesis that strong CAR signaling during early stages of lymphoid development drives T cell-to-ILC2 lineage diversion. We tested this by presentation of CD19 by stromal cells during lymphoid development in H1-CAR-low ATOs. We first generated a CD19-expressing ATO stromal line (MS5-hDLL4-CD19) and tested substitution of MS5-hDLL4 with this line at the EMO stage (day 14 to day 0), ATO stage (day 0 onward), or both stages (Figure 5F). We observed no effect on T cell development when CD19 was presented during the EMO stage only. In contrast, presentation of CD19 during the ATO stage or throughout the EMO and ATO stages resulted in a nearly complete block in T cell differentiation and robust ILC2 output, together with a striking increase in NK/ILC1-lineage cells characterized by subset expression of CD56 (Figures 5F, 5G, and S5B). These findings supported our findings from scRNA-seq that CAR-mediated T/ILC2 lineage bifurcation occurs between ATO days 0–7 rather than during earlier multilineage hematopoietic differentiation in EMOs and furthermore suggest that very strong, antigen-dependent CAR signaling enhances NK/ILC1 differentiation over CAR tonic signaling alone.

Using this finding, we also tested whether T cell-to-ILC lineage diversion could be driven by a strong TCR signal, independent of the costimulatory components of a CAR. We have shown previously that H1 ESCs transduced with the 1G4 A2/NY-ESO-1-restricted TCR[53] exhibited normal T cell differentiation.[9] However, we reasoned that TCRs transduced at the PSC stage are nonetheless prematurely expressed on the surface of lymphoid progenitor cells, given the broad expression of CD3 chains at these stages (Figures 4C and S4F), and, if activated, may disrupt T cell differentiation. To test this, hematopoietic progenitor cells derived in EMOs from 1G4 TCR-transduced H1 PSCs (H1–1G4) were reaggregated in ATOs with MS5-hDLL4 cells transduced with either an irrelevant (A2/MART1) or cognate (A2/ESO) peptide-major histocompatibility complex (pMHC). In this system, we indeed observed that T cell differentiation was blocked in the presence of the TCR cognate antigen, as seen by generation of DN and CD8αα+ cells, despite continued expression of the transgenic TCR (Figure S5C). As in the CAR system, exposure to antigen in ATOs resulted in a modestly expanded ILC2 compartment but a predominantly NK/ILC1-like population characterized by subset expression of CD56, CD8αα, and NK-associated receptors, including NKp46, CD94, CD16, and CD226 (Figure S5C). Thus, activation of transgenic CARs or TCRs during lymphoid development is sufficient to divert differentiation from T cell to ILC lineages.

Structural elements of CARs are also known to influence tonic and antigen-dependent CAR signaling, with modifications to the scFv, linker, hinge, TM, and signaling domains all shown to affect signaling strength and downstream T cell function.[4,7,8,54–57] We tested the effect of CAR structural variations that potentially lower tonic signaling on T versus ILC2 differentiation in ATOs. First, because the CD19 CAR used in the previous experiments contained a long, non-mutated IgG4 spacer with reported potential for antigen-independent ligation by Fc receptors,[54,58,59] we generated an H1 CAR line using an IgG4 “short hinge” (SH) CAR in which the CH2-CH3 spacer containing the Fc binding site was deleted but that was otherwise identical to the original CAR, containing CD28 TM and CD28ζ signaling domains (H1-CAR.SH.28TM.28ζ) (Figure 6A).[54] Deletion of the IgG4 CH2-CH3 spacer had no effect on ILC2-biased differentiation in ATOs (Figures 6B and 6C).

CD19 CARs incorporating 4–1BB signaling domains have been shown to have lower overall signaling strengths compared with CD28 signaling domain CARs.[6,7,60] Furthermore, the CD28 TM domain itself has been independently implicated in increased CAR signaling strength.[4,8,56] We altered these two elements by generating H1 lines with CD19 IgG4 "SH" CARs containing either CD28 TM and 4–1BBζ signaling domains (H1-CAR.SH.28TM.BBζ) or CD8α TM and 4–1BB ζ signaling domains (H1-CAR.SH.8αTM.BBζ) (Figure 6A). We generated PSC lines expressing high levels of these CARs to reduce the possibility of suboptimal CAR activation because of low expression. Accordingly, stably high surface CAR expression was seen for both 4–1BBζ CAR PSC lines (Figure S6A). Surprisingly, ATOs made using either 4–1BBζ CAR PSC line showed complete restoration of conventional CD3+TCRαβ+ CD8SP T cell differentiation with little to no ILC2 or NK/ILC1 output (Figures 6B and 6C). These data suggest that (1) the CD28 TM domain alone was insufficient to drive T cell-to-ILC2 diversion and (2) that, in contrast to CD28ζ CARs, tonic signaling levels of 4–1BBζ CARs are constrained enough to permit normal T cell development in ATOs. Supporting a mechanism of differential 4–1BBζ versus CD28ζ CAR signaling during early lymphoid development, phosphoflow analysis of day 4 ATOs showed constitutive CD3ζ and AKT phosphorylation as well as increased CD69 expression in CD7+ lymphoid precursors from CD28ζ but not 41BBζ CAR ATOs (Figures 6D and 6E).

Having verified preserved T cell differentiation in 4–1BBζ CAR ATOs, we tested whether this was due to an intrinsic inability of 4–1BBζ CARs to signal in early lymphoid precursors; for example, because of developmental lack of one or more 4–1BB signal transduction components. To test this, we again used stromal cell-presented CD19 beginning on day 0 in 4–1BBζ CAR ATOs. Indeed, provision of CD19 at this stage resulted in downregulation of surface CAR, a complete block in T cell development, and expansion of ILCs in CD8α TM (Figures 6F and 6G) and CD28 TM (Figure 6G) 4–1BBζ CAR ATOs. NK/ILC1-like cells were again predominant and showed partial expression of CD56, CD94, CD16, and other NK-associated markers (Figure S6B), similar to our observations in H1CAR-low ATOs reaggregated with CD19-expressing stromal cells and H1–1G4 ATOs reaggregated with A2/ESO-expressing stromal cells (Figures 5F, 5G, S5B, and S5C). We further verified the "group 1" ILC identity of these NK/ILC1-like cells by their expression of Tbet (with subset expression of Eomes) (Figure S6C), granzymes A and B, and production of IFNγ and TNF-α upon PMA/ionomycin stimulation (Figure S6D). Taken together, these data indicate that (1) 4–1BBζ CARs retain antigen-specific function during lymphocyte development, and (2) agonist signaling in 4–1BBζ CAR ATOs during early lymphoid development can direct CAR-T cell versus ILC output.

We next confirmed that CAR-T cells from 4–1BBζ CAR ATOs exhibited normal T cell function. T cells from 4–1BBζ CAR ATOs co-expressed conventional CD8αβ heterodimers and the mature T cells markers CD45RA and CD62L (Figure 7A). Stimulation with PMA/ionomycin revealed appropriate, polyfunctional production of IFNγ, TNF-α, and IL-2 as well as constitutive granzyme B expression (Figure 7B). CAR-T cells furthermore underwent antigen-specific cytokine release and degranulation in response to CD19+ but not CD19– Raji cells (Figure 7C). Finally, 4–1BBζ CD8SP CAR-T cells exhibited robust, antigen-dependent cytotoxicity against Raji cells in co-culture assays (Figure 7D).

Finally, because previous studies of PSC-derived CAR-T cell differentiation have used T cell-derived induced PSCs (T-iPSCs) as starting material,[3,61] we investigated the effect of the T-iPSC background on our central findings. Using a clonal T-iPSC line, we indeed found that transduction of our original CD19 CD28TM CD28ζ CAR led to prominent generation of CD200R+CD25+ ILC2s and modest expansion of CD56+NK/ILC1-like cells relative to parental T-iPSCs (Figure S7A). ILC phenotypes were conserved despite constitutive expression of the T-iPSC-derived TCR. Also consistent with our earlier findings in H1-CAR PSCs was that CD19 4–1BBζ CAR-transduced T-iPSCs gave rise to normal CAR-T cells without ILC2 or NK/ILC1 lineage diversion (Figure S7A). Furthermore, stromal cell presentation of CD19 during lymphoid development in 4–1BBζ CAR T-iPSC ATOs recapitulated loss of T cell differentiation and a predominantly NK/ILC1-like output, similar to that seen with CAR and TCR agonism in H1 ATOs. Overall, these findings indicate that the T cell origin and endogenous TCR expression of T-iPSCs are insufficient to override the dominant, inhibitory effect of strong CAR signaling on T cell development.

DISCUSSION

Our data reveal an unexpected effect of lentivirally expressed CD19-targeted CARs in diverting T cell differentiation to the closely related ILC2 lineage from PSCs. We conclude that CAR tonic signaling strength determines this lineage fate decision based on our observations that (1) CAR signaling in ATOs is antigen-independent because of the absence of cognate antigen expression in the system; (2) CD28ζ CARs exhibit an expression threshold over which T cell differentiation is diverted, and (3) CD19-targeted CARs containing the 4–1BB signaling domain, which exhibit lower tonic signaling, preserve T cell differentiation even at high levels of CAR expression.

Mechanistically, we establish that the effect of CAR signaling on T cell differentiation occurs at the earliest stages of lymphoid differentiation in ATOs. This was supported by our scRNA-seq analysis of early (day 0 to day 7) ATOs, which identified expansion of lineage-primed or lineage-committed ILC2 precursors in H1-CAR ATOs with a gene signature of TCR activation. Diversion of T cell to ILC differentiation by CAR activation is also supported by our observation that triggering antigen-dependent CAR activation during early lymphoid differentiation in the setting of low CAR tonic signaling CARs was sufficient to recapitulate T cell-to-ILC lineage diversion, an observation that also applied to transgenic TCR activation. Interestingly, antigen-induced CAR signaling prominently increased the proportion of NK/ILC1-like cells over that seen under high tonic CAR signaling conditions. The basis of this observation is unclear and may indicate mimicking of an endogenous NK/ILC1-specifying or supportive signal at very high levels of CAR/TCR activation. Analogous to this finding, cord blood (CB) CD34+ HSPCs transduced with a CD19 CD28ζ CAR preferentially generate NK-like cells *in vitro*,[62] a finding we independently verified in the CB ATO system (unpublished data). One reason for thismaybe,in contrastto PSCATOs, the presence of CD19+ cells during *in vitro* differentiation of CB HSPCs[10] driving antigen-dependent CAR activation and, thus, predominantly NK/ILC1-like differentiation from this cell source.

Taken together, our findings point to the importance of tuning CAR tonic signaling for generation of conventional CAR-T cells from PSCs using constitutively expressed lentiviral vectors. CAR-mediated diversion of T cell differentiation as the integration of CAR structure, expression level, developmental capacity of the CAR to signal, and potentially the platform used for T cell differentiation suggests that empirical optimization of each new CAR of interest may be required to achieve conventional CAR-T cell differentiation from PSCs. Moreover, our findings highlight the pitfalls of constitutive CAR expression and point to a need for exploring synthetic approaches, such as stage-specific or logic-gated CAR expression, to circumvent the effect of CARs on T cell development. This would be especially true in situations where the CAR's cognate antigen is present during T cell differentiation. An analogous, antigen-induced block in thymopoiesis has been demonstrated in mice transgenic for a TCR specific to an antigen expressed in the thymus, which furthermore developed T cell acute lymphoblastic leukemia as a result of persistent TCR activation in DN thymocytes.[63]

CAR-associated innate cell diversion has been observed previously by Themeli et al.,[3] who, using OP9-DL1 co-cultures, described cytotoxic "γδ-like" innate lymphoid differentiation from a T cell-derived iPSC (T-iPSC) line transduced with a CD19-targeted CD28ζ CAR. This innate phenotype was not CAR specific, however, because non-transduced T-iPSC cells displayed a similar phenotype, also reported by a contemporary group working with unmodified T-iPSCs.[64] This suggests that the PSC differentiation methods used at the time were not optimal for conventional T cell differentiation, confounding interpretation of the effect of CARs on T cell differentiation. A possible reason for the strong innate/NK-like output observed in earlier OP9-based systems versus ATOs may be lower levels or a shorter duration of DLL/Notch signaling in monolayer co-cultures compared with 3D ATO culture, given the known requirement for high Notch signaling in conventional T cell and ILC2 differentiation in mice and humans.[13–15] Working with a T-iPSC OP9-based differentiation model, Maeda et al.[65] showed that, despite predominant innate/NK-like differentiation, a minor population of conventional-appearing DP cells were generated that, upon TCR agonist engagement, adopted a CD8αβ+ mature T cell phenotype. Kawai et al.[66] and Minegawa et al.[67] further demonstrated the potential of CD3 and cytokine stimulation at the DP stage to support or expand CD8αβ+ T cells from OP9 and feeder-free PSC systems, but lymphocyte differentiation using T-iPSCs transduced with a glypican-3-specific CAR in this system still yielded cells with an NK-like ILC phenotype.[68] During the revision of this manuscript, two studies used these more refined monolayer culture systems to improve CAR-T cell generation from iPSCs. van der Stegen et al.[69] achieved T cell development when using a CD3ζ immunoreceptor tyrosine-based activation motif (ITAM)-mutated but not ITAM-intact CD19 CD28ζ CAR knocked into the *TRAC* locus, and Ueda et al.[70] achieved CD19 and glypican-3 CAR-T cell development using lentivirally transduced 4–1BBζ- but not CD28ζ-based CARs, corroborating our findings.

Recently, a study using the ATO system and T-iPSCs transduced with second-generation, CD19-targeted CD28ζ or 4–1BBζ CARs showed generation of CD8αβ+ CAR-T cells with potent, antigen-specific function.[61] In contrast to our findings, ILC2 differentiation was not observed. While the authors did not report CARs that blocked T cell differentiation, they noted that methylation of the lentiviral EF-1a promoter during T cell differentiation in ATOs

led to diminished CAR expression, a point of contrast to our CAR vectors, which used the *UBC* promoter and appeared to retain expression levels. CAR promoter methylation may therefore have resulted in lower CAR signaling levels permissive of T cell development and antigen-specific effector responses. While certain differences in mature CAR-T cell phenotypes were seen across these three recent studies and ours, collectively they illustrate different approaches to downmodulate CAR tonic signaling and point to the need for a systematic understanding of the "rules" of antigen receptor expression in PSCs to achieve conventional T cell differentiation.

Our findings also shed light on human T cell versus ILC2 lineage commitment, whose timing and cues are poorly understood. The modularity of the PSC ATO system and the ability to engineer the stromal cell component allowed us to show in this system that the T cell/ILC2 lineage bifurcation occurred during the first 7 days of lymphoid differentiation in ATOs and likely between day 0 and day 4, when distinct T cell and ILC precursor clusters had already emerged. Common thymic progenitors of T cells and ILCs have been identified,[13,14,71–73] reinforcing the close relationship between these lineages and suggesting the existence of lineage-differentiating microenvironmental cues that remain to be identified. Although non-physiological, CAR signaling in our model provides a potential starting point for identifying molecular regulators of T cell versus ILC2 differentiation. For example, in addition to the signature of TCR/CAR activation in ILC2 precursors, scRNA-seq also suggested activation of IL-4 signaling, a pathway implicated previously in ID2-mediated commitment of the ILC2 lineage in mice.[72] Whether this gene signature is confounded by transcriptional outputs from CAR signaling remains to be determined, but a future direction will be to test the hypothesis that CAR signaling is mimicking IL-4 or another physiological cytokine signal required for ILC2 commitment *in vivo*.

A final interesting observation from our study was the prominent CAR-specific upregulation of *ID3* in H1-CAR ILC2-primed precursors and mature CAR-ILC2 cells and its reciprocal pattern of expression with *ID2* in NK/ILC1 precursors. This contrasts with mouse ILC2 development, in which *Id2* plays a central role,[41,74] and more closely parallels induction of *Id3* by γδTCR signaling, which blocks differentiation to the conventional T cell lineage.[75] *ID3* upregulation also suggests a similarity between CAR-induced ILC2s and human neonatal ILC2s, which develop during fetal life and have been characterized by a higher *ID3*-to-*ID2* ratio than adult ILC2s.[48] Thus, a further intriguing possibility is that the ability of CARs to divert T cell to ILC2 differentiation from PSCs is a characteristic of fetal-like lymphocyte development, as we have shown previously for certain aspects of CD8 T cell development in PSC ATOs.[9]

In summary, our data provide a framework for understanding and applying CAR technology to T cell differentiation from PSCs and illuminates the potential to rationally control lymphoid-lineage fate decisions for developmental studies and future therapeutic applications.

Limitations of the study

We show that CAR-mediated diversion of lymphoid differentiation from T cell to ILC lineages is the product of multiple variables, including CAR structure, expression level

(dependent, in turn, on promoter strength and vector copy number), and the presence of cognate antigen, which together establish the level of CAR activation during lymphoid differentiation. Therefore, the specific CAR structures and expression levels we found to direct T cell or ILC differentiation in ATOs may not hold true for other CAR constructs or gene expression systems. In addition, levels of Notch ligand, IL-7, and other microenvironmental factors also important for lymphoid fate decisions may differ between the ATO system and other PSC-to-T cell differentiation models. Therefore, the effects of specific CARs will likely need to be determined empirically for different T cell differentiation methods.

STAR★METHODS

RESOURCE AVAILABILITY

Lead contact—Further information and requests for resources and reagents should be directed to and will be fulfilled by the Lead Contact, Christopher S. Seet (cseet@mednet.ucla.edu).

Materials availability—All unique and stable reagents generated in this study are available from the lead contact.

Data and code availability

- Both the bulk and single cell RNA-seq data have been deposited at GEO and are publicly available as of the date of publication. Accession numbers are listed in the key resources table.
- This paper does not report original code.
- Any additional information required to reanalyze the data reported in this paper is available from the lead contact upon request.

EXPERIMENTAL MODEL AND SUBJECT DETAILS

Cell lines—The MS5-hDLL4 cell line was generated as previously described.[9] The MS5-hDLL4-CD19 cell line was generated by further transduction with a lentiviral vector encoding truncated human CD19 and purified in bulk by FACS using an anti-CD19 antibody. CAR target cells RAJI-ffLuc-eGFP and RAJI-ffLuc-eGFP-CD19^{KO} cells were a gift from Yvonne Chen (UCLA). NALM6 cells were purchased from ATCC and for live imaging in Incucyte assays were transduced with a lentiviral vector encoding a nuclear-localized mKate2 fluorescent protein.[78]

Human pluripotent stem cell lines—The human embryonic stem cell (hESC) lines H1[27] (WiCell, Madison, WI) and ESI-017[35] (ESI BIO, Alameda, CA), and the N11 T-iPSC line (Cedars-Sinai iPSC Core, Los Angeles, CA) were maintained and expanded on Matrigel Growth Factor Reduced (GFR) Basement Membrane Matrix (BD Biosciences, Cat. 356231) in mTeSR Plus medium (Stem Cell Technologies, Cat. 100–0267). All CAR H1 and T-iPSC lines were generated by transduction of PSCs with VSV-G pseudotyped lentiviral vectors encoding different CARs with 2A-linked eGFP. Transduced PSCs were sorted by FACS

according to eGFP expression for either bulk use or clonal line derivation. Clonal lines were derived by plating FACS-sorted PSCs at limiting dilution on 10 cm Matrigel-coated plates until single colonies were visible, which were transferred with a pipet to 24-well plates for expansion and validation. Vector copy number (VCN) quantification on certain lines was performed by droplet digital PCR. Generation of the H1–1G4 TCR-transduced line was previously described.[9]

METHODS DETAILS

Generation and isolation of human embryonic mesodermal progenitors (hEMPs)—Mesoderm commitment was induced as previously described[9,79,80] with certain optimizations. Briefly, hESC cells were maintained on Matrigel-coated 6-well plates in mTeSR Plus complete medium. At day (D) −18, mesoderm induction was initiated in X-VIVO 15 medium (Lonza, Cat. 04–418Q) supplemented with recombinant human (rh) Activin A (10 ng/ml) (R&D Systems, Cat. 338-AC-010), rhBMP4 (10 ng/ml) (R&D Systems, Cat. 314-BP-010), rhVEGF (10 ng/ml) (R&D Systems, Cat. 298-VS-005), rhFGF (10 ng/ml) (R&D Systems, Cat. 233-FB-025), and ROCK inhibitor Y-27632 dihydrochloride (10 μM) (Tocris, Cat. 1254). hESCs were plated on Matrigel coated 6-well plates at 3×10^6 cells per well in 3ml. Medium was then changed daily with X-VIVO 15 supplemented with rhBMP4 (10 ng/ml), rhVEGF (10 ng/ml), and rhFGF (10 ng/ml). At D-14, cells were washed with PBS and detached with Accutase (Innovative Cell Technologies, Cat. AT-104) (1 mL per well, for 10 min at 37°C). Cells were harvested and hEMPs isolated by depletion of CD326+ cells by magnetic cell sorting (MACS) using CD326 (EpCAM) MicroBeads (Miltenyi, Cat. 130–061-101).

Pluripotent stem cell-derived embryonic mesoderm organoids (EMO) and reaggregated artificial thymic organoid (ATO) cultures—The sequential generation of hematoendothelial cells in EMOs followed by lymphocytes in ATOs is depicted in Figure 1A. First, EMOs were established by aggregating hEMPs with MS5-hDLL4 cells by centrifugation. Briefly, MS5-hDLL4 cells were harvested by trypsinization and resuspended in hematopoietic induction medium composed of EGM2 (Lonza Ref CC-4176) supplemented with ROCK inhibitor Y-27632 dihydrochloride (10μM) and TGFβRI inhibitor SB-431542 (10 μM) (Tocris Bioscience, Cat. 1614). At D-14, 5×10^5 MS5-hDLL4 cells were combined with 5×10^4 purified hEMP per EMO in 1.5 mL Eppendorf tubes and centrifuged at 300 *g* for 5 min at 4°C in a swinging bucket centrifuge. Supernatants were carefully removed, and the cell pellet resuspended by brief vortexing and suspension in hematopoietic induction medium at a volume of 6 μl per EMO. 6 μl of cells were then plated per EMO on 0.4 μm Millicell transwell inserts (EMD Millipore, Billerica, MA; Cat. PICM0RG50) (3 EMOs plated per insert) and placed in 6-well plates containing 1 mL of hematopoietic induction medium per well. Medium was changed completely every 2–3 days for 7 days. At D-7, medium was changed to EGM2 + 10 μM SB-431542 with 5 ng/ml rhTPO (R&D Systems, Cat. 288-TP), 5 ng/ml rhFLT3L (R&D Systems, Cat. 308-FK-025), and 50 ng/ml rhSCF (R&D Systems, Cat. 300–07). This medium was changed every 2–3 days for an additional 7 days (D-7 to D0).

At D0, EMOs were harvested into single cell suspensions in MACS buffer (PBS/0.5% bovine serum album/2mM EDTA) by mechanical dissociation for reaggregation into ATOs. Reaggregation served dual purposes of removing adherent, non-hematopoietic elements, resulting in more consistent lymphoid differentiation and permitting stage-specific manipulation of conditions at EMO and/or ATO stages, as described below. Briefly, EMOs were washed off culture inserts by pipetting and gently dissociated before passing through a 50 μm nylon strainer. Live, round, hematopoietic cells were counted with trypan blue and $1–5\times10^3$ live hematopoietic cells were reaggregated with 2.5×10^5 trypsinized MS5-hDLL4 cells per ATO. Lymphoid induction medium "RB27" (composed of RPMI 1640 (Corning, Manassas, VA), 4% B27 supplement (ThermoFisher Scientific, Grand Island, NY), 30 μM L-ascorbic acid 2-phosphate sesquimagnesium salt hydrate (Sigma-Aldrich, St. Louis, MO) reconstituted in PBS, 1% penicillin/streptomycin (Gemini Bio-Products, West Sacramento, CA), and 1% GlutaMAX (ThermoFisher Scientific, Grand Island, NY)) was supplemented with 10 ng/ml rhSCF, 5 ng/ml rhFLT3L, and 5 ng/ml rhIL-7 (R&D Systems, Cat. 207-IL-25). Media was changed completely every 3–4 days for 5–8 weeks. For downstream analysis, ATOs were harvested at the indicated timepoints by adding MACS buffer (PBS/0.5% bovine serum album/2mM EDTA) to each well and briefly disaggregating the ATO by pipetting with a 1 mL "P1000" pipet, followed by passage through a 50 μm nylon strainer. Cells were then analyzed by FACS or, for functional assays, debris and apoptotic cells were removed by MACS using the Dead Cell Removal Kit (Miltenyi, Auburn CA, Cat. 130–090-101) prior to use.

Lentiviral vectors and transduction—All CD19-targeted CARs used the scFv derived from FMC63.[30] Long or short IgG4 spacer/hinge domains were designed as previously described[58] followed by a human CD28 or CD8α transmembrane domain, a CD28 or 4–1BB costimulatory domain, and a CD3ζ intracellular signaling domain as previously described.[4,7] The codon optimized CAR coding sequences were cloned into the second generation pCCL lentiviral vector downstream of a ubiquitin C (UBC) promoter (gift of Donald Kohn, UCLA). A furin cleavage site, spacer, and 2A-linked eGFP fluorescent protein coding sequence was added downstream of CD3ζ.

Packaging and concentration of lentivirus particles was performed as previously described.[10] Briefly, 293T cells (ATCC) were co-transfected with lentiviral vector plasmid, pCMV-ΔR8.9, and pCAGGS-VSVG using TransIT-293 (Mirus Bio, Madison, WI, Cat. MIR 2700) for 17 hours followed by treatment with 10 mM sodium butyrate for 8 hours, followed by generation of cell supernatants in serum-free UltraCulture for 48 hours. Supernatants were concentrated by ultrafiltration using Amicon Ultra-15 100 KDa filters (EMD Millipore, Billerica, MA, Cat. UFC910024) at 4000 *g* for 40 minutes at °4C and stored as aliquots at −80C.

Flow cytometry—For phenotypic analysis, all surface flow cytometry stains were performed in PBS/0.5% BSA/2 mM EDTA for 20–30 min on ice. TruStain FcX (Biolegend, San Diego, CA) was added to all samples prior to antibody staining. DAPI was added to all samples prior to analysis for viability staining.

For intracellular transcription factor profiling, cells were stained for surface markers and Zombie Aqua Fixable Viability dye (Bio-legend, San Diego, CA) prior to fixation and permeabilization with True Nuclear Transcription Factor Staining kit (Biolegend, Cat. 424401) and intracellular stained with antibodies against GATA3, Eomes, Tbet, and RORγt.

For phosphoflow cytometry, day 4 ATO cells were collected, washed, and stained for surface markers and Zombie Aqua Fixable Viability dye (Biolegend, Cat. 423101) prior to fixation and permeabilization with an intracellular staining buffer kit (eBioscience, Cat. 88–8824-00) and intracellular stained with antibodies against corresponding phosphorylated proteins.

Analysis was performed on an LSRII Fortessa, and FACS sorting on ARIA or ARIA-H instruments (BD Biosciences, San Jose, CA) at the UCLA Broad Stem Cell Research Center Flow Cytometry Core. For all analyses, viable cells were gated based on the viability dye, and single cells were gated based on FSC-H, FSC-W, SSC-H, and SSC-W parameters. Anti-human antibody clones used for surface and intracellular staining were obtained from Biolegend (San Diego, CA): CD107a (H4A3), CD117 (104D2), CD127 (A019D5), CD16 (3G8), CD161 (HP-3G10), CD19 (H1B19), CD2 (RPA-2.10), CD22 (HIB22), CD200R (OX-108), CD235a (HI264), CD25 (BC96), CD294 (BM16), CD3 (UCHT1), CD34 (581), CD4 (RPA-T4), CD43 (CD43–10G7), CD45 (HI30), CD5 (UCHT2), CD56 (HCD56), CD7 (CD7–6B7), CD8α (SK1), CD94 (DX22), GM-CSF (BVD2–21C11), ICOS (C398.4A), interferon g (4S.B3), IL-13 (JES10–5A2), IL-2 (MQ1–17H12), IL-4 (MP4–25D2), IL-5 (JES1–39D10), NKG2D (1D11), NKp44 (P44–8), NKp46 (9E2), PD-1 (EH12.2H7), Tbet (4B10), TCRαβ (IP26), TNFα (Mab11), Biotin (1D4-C5), Invitrogen: Eomes (Clone WD1928), RORγt (Clone AFKJS-9), BD Biosciences (San Jose, CA): GATA3 (Clone L50–823), phosho-CD247 (pY142) (Clone K25–407.69), phospho-AKT (pS473) (Clone M89–61), and AcroBiosystems: Biotinylated Monoclonal Anti-FMC63 scFv Antibody. Anti-mouse CD29 (clone HMb1–1) was obtained from Biolegend. Flow cytometry data were analyzed with FlowJo software (Tree Star Inc.). A list of antibodies used is included in the key resources table.

***In vitro* proliferation assays—**H1-CAR ILC2s were isolated from week 5–9 ATOs as described above. For proliferation assays, up to 1×10^5 cells were plated in 200 μl AIM V (ThermoFisher Scientific, Cat. 12055091), 5% human AB serum (Gemini Bio, Cat. 100–512) with 20 ng/mL rhIL-2 (Peprotech) and 20 ng/mL rhIL-7 (Peprotech) plus indicated cytokines at 20 ng/mL (Peprotech) in the absence or presence of irradiated NALM6 cells at a 3:1 effector to target (E:T) ratio. Fresh cytokines were replenished at day 3 via half-media change, and cells were replated into larger wells when confluent, approximately every 2–3 days. Irradiated NALM6 cells were added again on day 7 of expansion. Cells were counted twice a week on a hemocytometer.

H1-CAR T cells were expanded at 5×10^5 cells/mL in AIM V (ThermoFisher Scientific, Cat. 12055091) supplemented with 5% human AB serum (Gemini Bio, Cat. 100–512), 5 ng/ml rhIL-7 (R&D), and 100 IU/ml rhIL-2 (Miltenyi Biotec, Cat. 130–097-748) with irradiated NALM6 cells added at a 3:1 E:T ratio 5 days prior to functional assays.

Intracellular cytokine assays—For intracellular cytokine detection, ILC2 or T cells were stimulated with PMA/ionomycin/protein transport inhibitor cocktail or control protein transport inhibitor cocktail (eBioscience, Cat 00–4975-93, Cat 00–4980-03, San Diego, CA) for 6 hours. APC-labeled CD107a antibody (Biolegend, clone H4A3) was added to wells at a 1:100 dilution for the final 2 hours of culture. Cells were collected, washed, and stained for surface markers and Zombie Aqua Fixable Viability dye (Biolegend, Cat. 423101) prior to fixation and permeabilization with an intracellular staining buffer kit (eBioscience, Cat. 88–8824-00) and intracellular staining with antibodies against corresponding cytokines. For antigen-specific CAR-T cytokine assays, T cells were expanded for 5 days with irradiated NALM6 cells as above and 1×10^5 CAR-T cells were co-cultured with RAJI or RAJI-CD19^{KO} cells at a 1:1 ratio for 6 hours with addition of APC anti-CD107a for the final 2 hours prior to fixation and staining as above.

***In vitro* ILC2 plasticity assay—**Week 6 H1-CAR ILC2 were purified from mechanically dissociated ATOs using the Dead Cell Removal Kit (Miltenyi, Auburn CA), followed by staining with PE-anti-CD8 and anti-PE MicroBeads (Miltenyi, Auburn CA) to deplete CD8+ T and NK/ILC1 cells. 1.5×10^5 ILC2-enriched cells were plated in 96-well U-bottom plates as per proliferation assays, above. For type 1 polarization, 20 ng/mL rhIL-12 (Peprotech) was added in addition to rhIL-7 and rhIL-2. For type 2 polarization, rhIL-25, rhIL-33, and rhTSLP were added in addition to rhIL-7 and rhIL-2 at 20 ng/ml each. On day 5, PMA/ionomycin with protein transport inhibitor cocktail (eBioscience, San Diego, CA) was added to each well for 6 hours. Cells were washed and stained for surface markers and Zombie Aqua (Biolegend, San Diego, CA) prior to fixation and permeabilization with an intracellular staining buffer kit (eBioscience, San Diego, CA) and intracellular staining with antibodies against IFNγ, TNFα, IL-5, and IL-13 (Biolegend, San Diego, CA).

***In vitro* cytotoxicity assays—**Tissue culture treated flat-bottom 96-well plates (Corning, Cat. 3904) were pre-coated with 50 μL/well poly-L-lysine (Sigma, Cat. P4832–50mL) for 1 h at room temperature followed by 3 washes with 200 μL PBS, followed by drying at room temperature for 2 hours. 1.5×10^4 RAJI cells transduced with nuclear-localized mKate2 as described above were plated per well in 100 μL RPMI 1640 with 10% FBS. Cells were incubated for 30 to 60 min to settle and adhere. CAR-T cells isolated from H1-CAR ATOs and expanded as above were added at a 1:1 E:T ratio in 100 μL RPMI 1640 with 10% FBS supplemented with 2X rhIL-7 (R&D) and rhIL-2 (Miltenyi, Cat. 130–097-748) for final concentrations of 5 ng/mL and 100 IU/mL, respectively. Control T cells from H1 ATOs were isolated from ATOs and used as CAR-negative controls. Triplicate wells were set up for each condition and live cell imaging was performed every 2 h for 3 days on an Incucyte Zoom instrument. Red fluorescence was evaluated at each timepoint using the manufacturer's software.

Bulk RNA sequencing—H1 ATO mature CD8SP T cells were FACS sorted as DAPI-CD3+TCRαβ+CD4-CD8αβ+CD45RA+ and H1-CAR-DN cells, containing ILC2s, as DAPI-eGFP+CD3-TCRαβ-CD8α-CD4- from week 6 ATOs. Biological triplicate samples were sorted from three independent experiments using a FACSAria II flow cytometer. Total RNA was isolated from $3–5\times10^4$ cells using the RNeasy Micro kit (QIAGEN) and 1.5 ng of

total RNA was input to generate sequencing libraries with SMARTer Stranded Total RNA-Seq (Pico) Kit (Clonetech, Cat. 635005). Paired-end 150 bp sequencing was performed on an Illumina HiSeq 3000. Raw sequence files were obtained, and quality checked using Illumina's proprietary software. The STAR ultrafast universal RNA-seq aligner v2.5.2b[81] was used to generate the genome index and perform paired-end alignments. Reads were aligned to a genome index that includes both the genome sequence (GRCh38 primary assembly) and the exon/intron structure of known gene models (Gencode v26 basic genome annotation). Alignment files were used to generate strand-specific, gene-level count summaries with STAR's built-in gene counter. Only protein-coding, long-noncoding, anti-sense and T-cell receptor genes in the Gencode v26 annotation were considered (98% of total counts on average). Independent filtering was applied as follows: genes with less than one count per sample on average, count outliers or low mappability were filtered out for downstream analysis.[82,83] Counts were normalized per-sample in units of FPKMs after correcting for gene mappable length and sample total counts. Differential expression analysis was performed with DESeq2.[83] Pair-wise differential expression was performed to classify genes as differentially expressed between any two cell types (Wald test adjusted p value < 1e-10, fold change >2). The volcano plot was made using the EnhancedVolcano package.[77]

Single cell RNA sequencing—Day 0, 4, and 7 ATOs were harvested into single cell suspensions in MACS buffer (PBS/0.5% bovine serum album/2mM EDTA) by mechanical dissociation. Live cells were first enriched with the Dead Cell Removal Kit (Miltenyi Biotec, Cat 130–019–101). Cells were then stained and FACS-sorted as DAPI- mouse CD29- (Biolegend, San Diego, CA) to deplete residual dead cells and MS5 stromal cells, respectively. 10X 3′ RNAseq library generation from sorted cells was performed by the UCLA Technology Center for Genomics and Bioinformatics (TCGB) Core using the 10X Genomics Chromium™ Controller Single Cell Sequencing System (10X Genomics, Pleasanton, CA), per the manufacturer's instructions and TCGB Core standard protocol. Libraries were sequenced on a NovaSeq 6000 S4 Flow cell (Illumina).

Data processing—Transcriptome data were mapped to the GRCh38 reference genome assembly with Cell Ranger (10X Genomics) and subjected to Seurat for pre-processing and normalization using SCTransfrom. Single-cell RNA analysis (including quality control, data normalization, dimension reduction, cluster detection, and differential expression testing) were performed using Seurat 4.0[76] in R following standard workflow. Cell cycle scores, percent of mitochondrial genes, and percent of ribosomal genes were assigned and regressed out during scaling. Normalized data were integrated based on identification of 'anchors' between pairs of datasets with reciprocal PCA. PCA was performed and significant PCs were selected based on the elbow of standard deviations of PCs. The first 20 PCs were used for calculation of UMAP (Uniform Manifold Approximation and Projection) and the neighborhood graph for clustering. The FindAllMarkers function was used to find specific genes for each cluster, which uses the Wilcoxon rank-sum test. Cell types were annotated based on the marker genes compared to canonical markers. Clusters expressing *CD7* and/or *IL7R* were defined as lymphoid cells and selected for further analysis. Lymphoid cells were then subjected to reclustering. To better appreciate heterogeneity within these cells, PCA

was recalculated in the lymphoid subset and PC of 20 was used for UMAP projection and clustering. Differential gene expression analyses were performed with the FindMarkers function using the Wilcoxon test with a log fold-change threshold of 0.25 and a minimum expression frequency of 0.1. Pathway analysis was performed using the Single Cell Pathway Analysis (SCPA) package in R.[84] Wikipathways were used as input gene sets using the msigdbr package.

Gene set enrichment analysis (GSEA)—T and ILC2 gene signatures were defined based on published single cell RNA-sequencing transcriptomes of human fetal hematopoietic cells. Raw transcript counts were obtained from GEO (GEO: GSE163587;[38]) and further processed using Seurat 4 in R. Single-cell data analysis (including quality control, data normalization, dimension reduction, clusters detection) were performed as described in Liu et al.[38] T and ILC2 lineage specific clusters were identified based on highly expressed specific markers in each cluster. Signature genes were defined by all the upregulated differentially expressed genes. Gene Set Enrichment Analysis (GSEA)[37] was performed using the GSEA software based on human T and ILC2 gene signatures between H1 SP8 T cells and H1-CAR DN ILC2 enriched cells.

QUANTIFICATION AND STATISTICAL ANALYSIS

Data are presented as mean ± standard deviation (s.d.) or mean ± standard error of the mean (SEM) as indicated. Statistical tests used are stated in each figure legend, adjusted p value significance was classified as such: *p < 0.5; **p < 0.01; ***p < 0.001; when tested. Statistical analyses were performed using GraphPad Prism software.

Supplementary Material

Refer to Web version on PubMed Central for supplementary material.

ACKNOWLEDGMENTS

We thank Felicia Codrea, Jessica Scholes, and Jeffrey Calimlim of the UCLA Broad Stem Cell Research Center Flow Cytometry Core for assistance with FACS and the UCLA Technology Center for Genomics & Bioinformatics (TCGB) Core for assistance with RNA sequencing. This work was supported by UCLA Broad Stem Cell Research Center fellowships (to S. Li and C.S.S.), a Tobacco-Related Disease Research Program predoctoral award (to S. Li), NIH 5T32HL086345-12 and 5T32HL066992-15 (to S.T.), the CIRM Bridges Program (to C.B.), NIH K08CA235525 (to C.S.S.), and a V Foundation scholar award (to C.S.S.).

REFERENCES

1. June CH, O'Connor RS, Kawalekar OU, Ghassemi S, and Milone MC (2018). CAR T cell immunotherapy for human cancer. Science 359, 1361–1365. 10.1126/science.aar6711. [PubMed: 29567707]
2. Montel-Hagen A, and Crooks GM (2019). From pluripotent stem cells toT cells. Exp. Hematol. 71, 24–31. 10.1016/j.exphem.2018.12.001. [PubMed: 30590093]
3. Themeli M, Kloss CC, Ciriello G, Fedorov VD, Perna F, Gonen M,and Sadelain M (2013). Generation of tumor-targeted human T lymphocytes from induced pluripotent stem cells for cancer therapy. Nat. Biotechnol. 31, 928–933. 10.1038/nbt.2678. [PubMed: 23934177]
4. Alabanza L, Pegues M, Geldres C, Shi V, Wiltzius JJW, Sievers SA, Yang S, and Kochenderfer JN (2017). Function of novel anti-CD19 chimeric antigen receptors with human variable

regions is affected by hinge and transmembrane domains. Mol. Ther. 25, 2452–2465. 10.1016/j.ymthe.2017.07.013. [PubMed: 28807568]

5. Gomes-Silva D, Mukherjee M, Srinivasan M, Krenciute G, Dakhova O, Zheng Y, Cabral JMS, Rooney CM, Orange JS, Brenner MK, and Mamonkin M (2017). Tonic 4–1BB costimulation in chimeric antigen receptors impedes T cell survival and is vector-dependent. Cell Rep. 21, 17–26. 10.1016/j.celrep.2017.09.015. [PubMed: 28978471]
6. Li W, Guo L, Rathi P, Marinova E, Gao X, Wu MF, Liu H, Dotti G,Gottschalk S, Metelitsa LS, and Heczey A (2017). Redirecting T cells to glypican-3 with 4–1BB zeta chimeric antigen receptors results in Th1 polarization and potent antitumor activity. Hum. Gene Ther. 28, 437–448. 10.1089/hum.2016.025. [PubMed: 27530312]
7. Long AH, Haso WM, Shern JF, Wanhainen KM, Murgai M, Ingaramo M, Smith JP, Walker AJ, Kohler ME, Venkateshwara VR, et al. (2015). 4–1BB costimulation ameliorates T cell exhaustion induced by tonic signaling of chimeric antigen receptors. Nat. Med. 21, 581–590. 10.1038/nm.3838. [PubMed: 25939063]
8. Majzner RG, Rietberg SP, Sotillo E, Dong R, Vachharajani VT, Labanieh L, Myklebust JH, Kadapakkam M, Weber EW, Tousley AM, et al. (2020). Tuning the antigen density requirement for CAR T-cell activity. Cancer Discov. 10, 702–723. 10.1158/2159-8290.Cd-19-0945. [PubMed: 32193224]
9. Montel-Hagen A, Seet CS, Li S, Chick B, Zhu Y, Chang P, Tsai S,Sun V, Lopez S, Chen HC, et al. (2019). Organoid-induced differentiation of conventional T cells from human pluripotent stem cells. Cell Stem Cell 24, 376–389.e378. 10.1016/j.stem.2018.12.011. [PubMed: 30661959]
10. Seet CS,He C,Bethune MT, Li S, Chick B, Gschweng EH, Zhu Y,Kim K, Kohn DB, Baltimore D, et al. (2017). Generation of mature T cells from human hematopoietic stem and progenitor cells in artificial thymic organoids. Nat. Methods 14, 521–530. 10.1038/nmeth.4237. [PubMed: 28369043]
11. Artis D, and Spits H (2015). The biology of innate lymphoid cells. Nature517, 293–301. 10.1038/nature14189.
12. Vivier E, Artis D, Colonna M, Diefenbach A, Di Santo JP, Eberl G,Koyasu S, Locksley RM, McKenzie ANJ, Mebius RE, et al. (2018). Innate lymphoid cells: 10 Years on. Cell 174, 1054–1066. 10.1016/j.cell.2018.07.017. [PubMed: 30142344]
13. Ferreira ACF, Szeto ACH, Heycock MWD, Clark PA, Walker JA,Crisp A, Barlow JL, Kitching S, Lim A, Gogoi M, et al. (2021). RORα is a critical checkpoint for T cell and ILC2 commitment in the embryonic thymus. Nat. Immunol. 22, 166–178. 10.1038/s41590-020-00833-w. [PubMed: 33432227]
14. Gentek R, Munneke JM, Helbig C, Blom B, Hazenberg MD, Spits H, and Amsen D (2013). Modulation of signal strength switches Notch from an inducer of T cells to an inducer of ILC2. Front. Immunol. 4, 334. 10.3389/fimmu.2013.00334. [PubMed: 24155745]
15. Koga S, Hozumi K, Hirano KI, Yazawa M, Terooatea T, Minoda A,Nagasawa T, Koyasu S, and Moro K (2018). Peripheral PDGFRα(+) gp38(+) mesenchymal cells support the differentiation of fetal liver-derived ILC2. J. Exp. Med. 215, 1609–1626.10.1084/jem.20172310. [PubMed: 29728440]
16. Califano D, Cho JJ, Uddin MN, Lorentsen KJ, Yang Q, Bhandoola A, Li H, and Avram D (2015). Transcription factor Bcl11b controls identity and function of mature type 2 innate lymphoid cells. Immunity 43, 354–368. 10.1016/j.immuni.2015.07.005. [PubMed: 26231117]
17. Hoyler T, Klose CS, Souabni A, Turqueti-Neves A, Pfeifer D, Rawlins EL, Voehringer D, Busslinger M, and Diefenbach A (2012). The transcription factor GATA-3 controls cell fate and maintenance of type 2 innate lymphoid cells. Immunity 37, 634–648. 10.1016/j.immuni.2012.06.020. [PubMed: 23063333]
18. Klein Wolterink RG, Serafini N, van Nimwegen M, Vosshenrich CA, de Bruijn MJ, Fonseca Pereira D, Veiga Fernandes H, Hendriks RW, and Di Santo JP (2013). Essential, dose-dependent role for the transcription factor Gata3 in the development of IL-5+ and IL-13+ type 2 innate lymphoid cells. Proc. Natl. Acad. Sci. USA 110, 10240–10245. 10.1073/pnas.1217158110. [PubMed: 23733962]
19. Walker JA, Oliphant CJ, Englezakis A, Yu Y, Clare S, Rodewald HR, Belz G, Liu P, Fallon PG, and McKenzie AN (2015). Bcl11b is essential for group 2 innate lymphoid cell development. J. Exp. Med.212, 875–882. 10.1084/jem.20142224. [PubMed: 25964370]

20. Yagi R, Zhong C, Northrup DL, Yu F, Bouladoux N, Spencer S, Hu G, Barron L, Sharma S, Nakayama T, et al. (2014). The transcription factor GATA3 is critical for the development of all IL-7Rα-expressing innate lymphoid cells. Immunity 40, 378–388. 10.1016/j.immuni.2014.01.012. [PubMed: 24631153]
21. Yang Q, Monticelli LA, Saenz SA, Chi AW, Sonnenberg GF, Tang J, De Obaldia ME, Bailis W, Bryson JL, Toscano K, et al. (2013). T cell factor 1 is required for group 2 innate lymphoid cell generation. Immunity 38, 694–704. 10.1016/j.immuni.2012.12.003. [PubMed: 23601684]
22. Yu Y, Wang C, Clare S, Wang J, Lee SC, Brandt C, Burke S, Lu L, He D, Jenkins NA, et al. (2015). The transcription factor Bcl11b is specifically expressed in group 2 innate lymphoid cells and is essential for their development. J. Exp. Med. 212, 865–874. 10.1084/jem.20142318. [PubMed: 25964371]
23. Morrow MA, Mayer EW, Perez CA, Adlam M, and Siu G (1999). Overexpression of the Helix-Loop-Helix protein Id2 blocks T cell development at multiple stages. Mol. Immunol. 36, 491–503. 10.1016/s0161-5890(99)00071-1. [PubMed: 10475604]
24. Xu W, Cherrier DE, Chea S, Vosshenrich C, Serafini N, Petit M, Liu P, Golub R, and Di Santo JP (2019). An Id2RFP-reporter mouse redefines innate lymphoid cell precursor potentials. Immunity 50, 1054–1068.e1053. 10.1016/j.immuni.2019.02.022. [PubMed: 30926235]
25. Boos MD, Yokota Y, Eberl G, and Kee BL (2007). Mature naturalkiller cell and lymphoid tissue–inducing cell development requires Id2-mediated suppression of E protein activity. J. Exp. Med. 204, 1119–1130. 10.1084/jem.20061959. [PubMed: 17452521]
26. Zook EC, Li Z-Y, Xu Y, Pooter R.F.d., Verykokakis M, Beaulieu A,Lasorella A, Maienschein-Cline M, Sun JC, Sigvardsson M, and Kee BL (2018). Transcription factor ID2 prevents E proteins from enforcing a naı¨ve T lymphocyte gene program during NK cell development. Science Immunology 3, eaao2139. 10.1126/sciimmunol.aao2139.
27. Thomson JA, Itskovitz-Eldor J, Shapiro SS, Waknitz MA, Swiergiel JJ, Marshall VS, and Jones JM (1998). Embryonic stem cell lines derived from human blastocysts. Science 282, 1145–1147. 10.1126/science.282.5391.1145. [PubMed: 9804556]
28. Kochenderfer JN, Feldman SA, Zhao Y, Xu H, Black MA, Morgan RA, Wilson WH, and Rosenberg SA (2009). Construction and preclinical evaluation of an anti-CD19 chimeric antigen receptor. J. Immunother. 32, 689–702. 10.1097/CJI.0b013e3181ac6138. [PubMed: 19561539]
29. Kowolik CM, Topp MS, Gonzalez S, Pfeiffer T, Olivares S, Gonzalez N, Smith DD, Forman SJ, Jensen MC, and Cooper LJ (2006). CD28 costimulation provided through a CD19-specific chimeric antigen receptor enhances in vivo persistence and antitumor efficacy of adoptively transferred T cells. Cancer Res. 66, 10995–11004. 10.1158/0008-5472.Can-06-0160. [PubMed: 17108138]
30. Nicholson IC, Lenton KA, Little DJ, Decorso T, Lee FT, Scott AM, Zola H, and Hohmann AW (1997). Construction and characterisation of a functional CD19 specific single chain Fv fragment for immunotherapy of B lineage leukaemia and lymphoma. Mol. Immunol. 34, 1157–1165. 10.1016/s0161-5890(97)00144-2. [PubMed: 9566763]
31. McFarland AP, Yalin A, Wang SY, Cortez VS, Landsberger T, Sudan R, Peng V, Miller HL, Ricci B, David E, et al. (2021). Multi-tissue single-cell analysis deconstructs the complex programs of mouse natural killer and type 1 innate lymphoid cells in tissues and circulation. Immunity 54, 1320–1337.e1324. 10.1016/j.immuni.2021.03.024. [PubMed: 33945787]
32. Seillet C, Brossay L, and Vivier E (2021). Natural killers or ILC1s? Thatis the question. Curr. Opin. Immunol. 68, 48–53. 10.1016/j.coi.2020.08.009. [PubMed: 33069142]
33. Yudanin NA, Schmitz F, Flamar AL, Thome JJC, Tait Wojno E,Moeller JB, Schirmer M, Latorre IJ, Xavier RJ, Farber DL, et al. (2019). Spatial and temporal mapping of human innate lymphoid cells reveals elements of tissue specificity. Immunity 50, 505–519.e504. 10.1016/j.immuni.2019.01.012. [PubMed: 30770247]
34. Hernández DC, Juelke K, Müller NC, Durek P, Ugursu B, Mashreghi MF, Rückert T, and Romagnani C. (2021). An in vitro platform supports generation of human innate lymphoid cells from CD34(+) hematopoietic progenitors that recapitulate ex vivo identity. Immunity 54, 2417–2432.e2415. 10.1016/j.immuni.2021.07.019. [PubMed: 34453879]

35. Crook JM, Peura TT, Kravets L, Bosman AG, Buzzard JJ, Horne R, Hentze H, Dunn NR, Zweigerdt R, Chua F, et al. (2007). The generation of six clinical-grade human embryonic stem cell lines. Cell Stem Cell 1, 490–494. 10.1016/j.stem.2007.10.004. [PubMed: 18938745]
36. Mjösberg JM, Trifari S, Crellin NK, Peters CP, van Drunen CM, Piet B, Fokkens WJ, Cupedo T, and Spits H (2011). Human IL-25- and IL-33-responsive type 2 innate lymphoid cells are defined by expression of CRTH2 and CD161. Nat. Immunol. 12, 1055–1062. 10.1038/ni.2104. [PubMed: 21909091]
37. Subramanian A, Tamayo P, Mootha VK, Mukherjee S, Ebert BL,Gillette MA, Paulovich A, Pomeroy SL, Golub TR, Lander ES, and Mesirov JP (2005). Gene set enrichment analysis: A knowledge-based approach for interpreting genome-wide expression profiles. Proc. Natl. Acad. Sci. USA 102, 15545–15550. 10.1073/pnas.0506580102. [PubMed: 16199517]
38. Liu C, Gong Y, Zhang H, Yang H, Zeng Y, Bian Z, Xin Q, Bai Z,Zhang M, He J, et al. (2021). Delineating spatiotemporal and hierarchical development of human fetal innate lymphoid cells. Cell Res. 31, 1106–1122. 10.1038/s41422-021-00529-2. [PubMed: 34239074]
39. Mazzurana L, Czarnewski P, Jonsson V, Wigge L, Ringnér M, Williams TC, Ravindran A, Björklund Å K, Säfholm J, Nilsson G, et al. (2021). Tissue-specific transcriptional imprinting and heterogeneity in human innate lymphoid cells revealed by full-length single-cell RNA-sequencing. Cell Res. 31, 554–568. 10.1038/s41422-020-00445-x. [PubMed: 33420427]
40. Howard E, Hurrell BP, Helou DG, Quach C, Painter JD, Shafiei-Jahani P, Fung M, Gill PS, Soroosh P, Sharpe AH, and Akbari O (2021). PD-1 blockade on tumor microenvironment-resident ILC2s promotes TNF-α production and restricts progression of metastatic melanoma. Front. Immunol. 12, 733136. 10.3389/fimmu.2021.733136.
41. Moro K, Yamada T, Tanabe M, Takeuchi T, Ikawa T, Kawamoto H,Furusawa J, Ohtani M, Fujii H, and Koyasu S (2010). Innate production of T(H)2 cytokines by adipose tissue-associated c-Kit(+)Sca-1(+) lymphoid cells. Nature 463, 540–544. 10.1038/nature08636. [PubMed: 20023630]
42. Bal SM, Bernink JH, Nagasawa M, Groot J, Shikhagaie MM, Go-lebski K, van Drunen CM, Lutter R, Jonkers RE, Hombrink P, et al. (2016). IL-1β, IL-4 and IL-12 control the fate of group 2 innate lymphoid cells in human airway inflammation in the lungs. Nat. Immunol. 17, 636–645. 10.1038/ni.3444. [PubMed: 27111145]
43. Camelo A, Rosignoli G, Ohne Y, Stewart RA, Overed-Sayer C, Sleeman MA, and May RD (2017). IL-33, IL–25, and TSLP induce a distinct phenotypic and activation profile in human type 2 innate lymphoid cells. Blood Adv 1, 577–589. 10.1182/bloodadvances.2016002352. [PubMed: 29296700]
44. Lim AI, Menegatti S, Bustamante J, Le Bourhis L, Allez M, Rogge L, Casanova JL, Yssel H, and Di Santo JP (2016). IL-12 drives functional plasticity of human group 2 innate lymphoid cells. J. Exp. Med. 213, 569–583. 10.1084/jem.20151750. [PubMed: 26976630]
45. Ohne Y, Silver JS, Thompson-Snipes L, Collet MA, Blanck JP,Cantarel BL, Copenhaver AM, Humbles AA, and Liu YJ (2016). IL-1 is a critical regulator of group 2 innate lymphoid cell function and plasticity. Nat. Immunol. 17, 646–655. 10.1038/ni.3447. [PubMed: 27111142]
46. Tufa DM, Yingst AM, Trahan GD, Shank T, Jones D, Shim S,Lake J, Winkler K, Cobb L, Woods R, et al. (2020). Human innate lymphoid cell precursors express CD48 that modulates ILC differentiation through 2B4 signaling. Sci Immunol 5. 10.1126/sciimmunol.aay4218.
47. Wang HC, Qian L, Zhao Y, Mengarelli J, Adrianto I, Montgomery CG, Urban JF Jr., Fung KM, and Sun XH (2017). Downregulation of E protein activity augments an ILC2 differentiation program in the thymus. J. Immunol. 198, 3149–3156. 10.4049/jimmunol.1602009. [PubMed: 28258196]
48. Bennstein SB, Scherenschlich N, Weinhold S, Manser AR, Noll A,Raba K, Kögler G, Walter L, and Uhrberg M (2021). Transcriptional and functional characterization of neonatal circulating innate lymphoid cells. Stem Cells Transl Med 10, 867–882. 10.1002/sctm.20-0300. [PubMed: 33475258]
49. Esensten JH, Helou YA, Chopra G, Weiss A, and Bluestone JA(2016). CD28 costimulation: From mechanism to therapy. Immunity 44, 973–988. 10.1016/j.immuni.2016.04.020. [PubMed: 27192564]

50. Eyquem J, Mansilla-Soto J, Giavridis T, van der Stegen SJ, Hamieh M, Cunanan KM, Odak A, Gönen M, and Sadelain M (2017). Targeting a CAR to the TRAC locus with CRISPR/Cas9 enhances tumour rejection. Nature 543, 113–117. 10.1038/nature21405. [PubMed: 28225754]
51. Ho JY, Wang L, Liu Y, Ba M, Yang J, Zhang X, Chen D, Lu P, andLi J (2021). Promoter usage regulating the surface density of CAR molecules may modulate the kinetics of CAR-T cells in vivo. Mol Ther Methods Clin Dev 21, 237–246. 10.1016/j.omtm.2021.03.007. [PubMed: 33869653]
52. Li W, Qiu S, Chen J, Jiang S, Chen W, Jiang J, Wang F, Si W, Shu Y, Wei P, et al. .(2020).Chimeric antigen receptor designed to prevent ubiquitination and downregulation showed durable antitumor efficacy. Immunity 53, 456–470.e456. 10.1016/j.immuni.2020.07.011. [PubMed: 32758419]
53. Robbins PF, Li YF, El-Gamil M, Zhao Y, Wargo JA, Zheng Z, Xu H, Morgan RA, Feldman SA, Johnson LA, et al. (2008). Single and dual amino acid substitutions in TCR CDRs can enhance antigen-specific T cell functions. J. Immunol. 180, 6116–6131. 10.4049/jimmunol.180.9.6116. [PubMed: 18424733]
54. Hudecek M, Lupo-Stanghellini MT, Kosasih PL, Sommermeyer D, Jensen MC, Rader C, and Riddell SR (2013). Receptor affinity and extracellular domain modifications affect tumor recognition by ROR1-specific chimeric antigen receptor T cells. Clin. Cancer Res. 19, 3153–3164. 10.1158/1078-0432.Ccr-13-0330. [PubMed: 23620405]
55. Leick MB, Silva H, Scarfò I, Larson R, Choi BD, Bouffard AA, Gallagher K, Schmidts A, Bailey SR, Kann MC, et al. (2022). Non-cleavable hinge enhances avidity and expansion of CAR-T cells for acute myeloid leukemia. Cancer Cell 40, 494–508. 10.1016/j.ccell.2022.04.001. [PubMed: 35452603]
56. Muller YD, Nguyen DP, Ferreira LMR, Ho P, Raffin C, Valencia RVB, Congrave-Wilson Z, Roth TL, Eyquem J, Van Gool F, et al. (2021). The CD28-transmembrane domain mediates chimeric antigen receptor heterodimerization with CD28. Front. Immunol. 12, 639818. 10.3389/fimmu.2021.639818.
57. Zhao Z, Condomines M, van der Stegen SJC, Perna F, Kloss CC, Gunset G, Plotkin J, and Sadelain M (2015). Structural design of engineered costimulation determines tumor rejection kinetics and persistence of CAR T cells. Cancer Cell 28, 415–428. 10.1016/j.ccell.2015.09.004. [PubMed: 26461090]
58. Hudecek M, Sommermeyer D, Kosasih PL, Silva-Benedict A, Liu L,Rader C, Jensen MC, and Riddell SR (2015). The nonsignaling extracellular spacer domain of chimeric antigen receptors is decisive for in vivo antitumor activity. Cancer Immunol Res 3, 125–135. 10.1158/2326-6066.Cir-14-0127. [PubMed: 25212991]
59. Jonnalagadda M, Mardiros A, Urak R, Wang X, Hoffman LJ, Bernanke A, Chang WC, Bretzlaff W, Starr R, Priceman S, et al. (2015). Chimeric antigen receptors with mutated IgG4 Fc spacer avoid fc receptor binding and improve T cell persistence and antitumor efficacy. Mol. Ther. 23, 757–768. 10.1038/mt.2014.208. [PubMed: 25366031]
60. Kawalekar OU, RS OC, Fraietta JA, Guo L, McGettigan SE, Posey AD Jr., Patel PR, Guedan S, Scholler J, Keith B, et al. (2016). Distinct signaling of coreceptors regulates specific metabolism pathways and impacts memory development in CAR T cells. Immunity 44, 712. 10.1016/j.immuni.2016.02.023.
61. Wang Z, McWilliams-Koeppen HP, Reza H, Ostberg JR, Chen W,Wang X, Huynh C, Vyas V, Chang WC, Starr R, et al. (2022). 3D-organoid culture supports differentiation of human CAR(+) iPSCs into highly functional CAR T cells. Cell Stem Cell 29, 515–527. 10.1016/j.stem.2022.02.009. [PubMed: 35278370]
62. Maluski M, Ghosh A, Herbst J, Scholl V, Baumann R, Huehn J, Geffers R, Meyer J, Maul H, Eiz-Vesper B, et al. (2019). Chimeric antigen receptor-induced BCL11B suppression propagates NK-like cell development. J. Clin. Invest. 129, 5108–5122. 10.1172/jci126350. [PubMed: 31479431]
63. Cui Y, Onozawa M, Garber HR, Samsel L, Wang Z, McCoy JP,Burkett S, Wu X, Aplan PD, and Mackall CL (2015). Thymic expression of a T-cell receptor targeting a tumor-associated antigen coexpressed in the thymus induces T-ALL. Blood 125, 2958–2967. 10.1182/blood-2014-10-609271. [PubMed: 25814528]
64. Nishimura T, Kaneko S, Kawana-Tachikawa A, Tajima Y, Goto H, Zhu D, Nakayama-Hosoya K, Iriguchi S, Uemura Y, Shimizu T, et al. (2013). Generation of rejuvenated antigen-specific

T cells by reprogramming to pluripotency and redifferentiation. Cell Stem Cell 12, 114–126. 10.1016/j.stem.2012.11.002. [PubMed: 23290140]

65. Maeda T, Nagano S, Ichise H, Kataoka K, Yamada D, Ogawa S,Koseki H, Kitawaki T, Kadowaki N, Takaori-Kondo A, et al. (2016). Regeneration of CD8αβ T cells from T-cell-derived iPSC imparts potent tumor antigen-specific cytotoxicity. Cancer Res. 76, 6839–6850. 10.1158/0008-5472.Can-16-1149. [PubMed: 27872100]
66. Kawai Y, Kawana-Tachikawa A, Kitayama S, Ueda T, Miki S, Watanabe A, and Kaneko S (2021). Generation of highly proliferative, rejuvenated cytotoxic T cell clones through pluripotency reprogramming for adoptive immunotherapy. Mol. Ther. 29, 3027–3041. 10.1016/j.ymthe.2021.05.016. [PubMed: 34023508]
67. Minagawa A, Yoshikawa T, Yasukawa M, Hotta A, Kunitomo M, Iriguchi S, Takiguchi M, Kassai Y, Imai E, Yasui Y, et al. (2018). Enhancing T cell receptor stability in rejuvenated iPSC-derived T cells improves their use in cancer immunotherapy. Cell Stem Cell 23, 850–858.e854. 10.1016/j.stem.2018.10.005. [PubMed: 30449714]
68. Ueda T, Kumagai A, Iriguchi S, Yasui Y, Miyasaka T, Nakagoshi K, Nakane K, Saito K, Takahashi M, Sasaki A, et al. (2020). Non-clinical efficacy, safety and stable clinical cell processing of induced pluripotent stem cell-derived anti-glypican-3 chimeric antigen receptor-expressing natural killer/innate lymphoid cells. Cancer Sci. 111, 1478–1490. 10.1111/cas.14374. [PubMed: 32133731]
69. van der Stegen SJC, Lindenbergh PL, Petrovic RM, Xie H, Diop MP, Alexeeva V, Shi Y, Mansilla-Soto J, Hamieh M, Eyquem J, et al. (2022). Generation of T-cell-receptor-negative CD8αβ-positive CAR T cells from T-cell-derived induced pluripotent stem cells. Nat. Biomed. Eng. 6, 1284–1297. 10.1038/s41551-022-00915-0. [PubMed: 35941192]
70. Ueda T, Shiina S, Iriguchi S, Terakura S, Kawai Y, Kabai R, Sakamoto S, Watanabe A, Ohara K, Wang B, et al. (2022). Optimization of the proliferation and persistency of CAR T cells derived from human induced pluripotent stem cells. Nat. Biomed. Eng. 7, 24–37. 10.1038/s41551-022-00969-0. [PubMed: 36509913]
71. Elsaid R, Meunier S, Burlen-Defranoux O, Soares-da-Silva F, Perchet T, Iturri L, Freyer L, Vieira P, Pereira P, Golub R, et al. (2021). A wave of bipotent T/ILC-restricted progenitors shapes the embryonic thymus microenvironment in a time-dependent manner. Blood 137, 1024–1036. 10.1182/blood.2020006779. [PubMed: 33025012]
72. Qian L, Bajana S, Georgescu C, Peng V, Wang HC, Adrianto I, Colonna M, Alberola-Ila J, Wren JD, and Sun XH (2019). Suppression of ILC2 differentiation from committed T cell precursors by E protein transcription factors. J. Exp. Med. 216, 884–899. 10.1084/jem.20182100. [PubMed: 30898894]
73. Wong SH, Walker JA, Jolin HE, Drynan LF, Hams E, Camelo A,Barlow JL, Neill DR, Panova V, Koch U, et al. (2012). Transcription factor RORα is critical for nuocyte development. Nat. Immunol. 13, 229–236. 10.1038/ni.2208. [PubMed: 22267218]
74. Miyazaki M, Miyazaki K, Chen K, Jin Y, Turner J, Moore AJ, Saito R, Yoshida K, Ogawa S, Rodewald HR, et al. (2017). The E-id protein Axis specifies adaptive lymphoid cell identity and suppresses thymic innate lymphoid cell development. Immunity 46, 818–834.e814. 10.1016/j.immuni.2017.04.022. [PubMed: 28514688]
75. Fahl SP, Contreras AV, Verma A, Qiu X, Harly C, Radtke F, Zúñiga-Pflücker JC, Murre C, Xue HH, Sen JM, and Wiest DL (2021). The E protein-TCF1 axis controls γδ T cell development and effector fate. CellRep. 34, 108716. 10.1016/j.celrep.2021.108716.
76. Hao Y, Hao S, Andersen-Nissen E, Mauck WM 3rd, Zheng S, Butler A, Lee MJ, Wilk AJ, Darby C, Zager M, et al. (2021). Integrated analysis of multimodal single-cell data. Cell 184, 3573–3587.e3529. 10.1016/j.cell.2021.04.048. [PubMed: 34062119]
77. Blighe K, Rana S, Turkes E, Ostendorf B, Grioni A, and Lewis M (2022). EnhancedVolcano: Publication-Ready Volcano Plots with Enhanced Colouring and Labeling. 10.18129/B9.bioc.EnhancedVolcano.
78. Lanigan TM, Rasmussen SM, Weber DP, Athukorala KS, Campbell PL, Fox DA, and Ruth JH (2020). Real time visualization of cancer cell death, survival and proliferation using fluorochrome-transfected cells in an IncuCyte(®) imaging system. J. Biol. Methods 7, e133. 10.14440/jbm.2020.323. [PubMed: 32577423]

79. Chin CJ, Cooper AR, Lill GR, Evseenko D, Zhu Y, He CB,Casero D, Pellegrini M, Kohn DB, and Crooks GM (2016). Genetic tagging during human mesoderm differentiation reveals tripotent lateral plate mesodermal progenitors. Stem Cell. 34, 1239–1250. 10.1002/stem.2351.

80. Evseenko D, Zhu Y, Schenke-Layland K, Kuo J, Latour B, Ge S,Scholes J, Dravid G, Li X, MacLellan WR, and Crooks GM (2010). Mapping the first stages of mesoderm commitment during differentiation of human embryonic stem cells. Proc. Natl. Acad. Sci. USA 107, 13742–13747. 10.1073/pnas.1002077107. [PubMed: 20643952]

81. Dobin A, Davis CA, Schlesinger F, Drenkow J, Zaleski C, Jha S, Batut P, Chaisson M, and Gingeras TR (2013). STAR: Ultrafast universal RNA-seq aligner. Bioinformatics 29, 15–21. 10.1093/bioinformatics/bts635. [PubMed: 23104886]

82. Casero D, Sandoval S, Seet CS, Scholes J, Zhu Y, Ha VL, Luong A, Parekh C, and Crooks GM (2015). Long non-coding RNA profiling of human lymphoid progenitor cells reveals transcriptional divergence of B cell and T cell lineages. Nat. Immunol. 16, 1282–1291. 10.1038/ni.3299. [PubMed: 26502406]

83. Love MI, Huber W, and Anders S (2014). Moderated estimation of fold change and dispersion for RNA-seq data with DESeq2. Genome Biol. 15, 550. 10.1186/s13059-014-0550-8. [PubMed: 25516281]

84. Bibby JA, Agarwal D, Freiwald T, Kunz N, Merle NS, West EE,Larochelle A, Chinian F, Mukherjee S, Afzali B, et al. (2022). Systematic Single Cell Pathway Analysis (SCPA) reveals novel pathways engaged during early T cell activation. Preprint at bioRxiv. 10.1101/2022.02.07.478807.

Highlights

- Tonic CAR signaling diverts T cell differentiation to the ILC lineage from hPSCs
- CAR activation during early lymphoid development enriches for ILC2 precursors
- Antigen-mediated CAR activation during development enhances NK/ILC1 output
- Lower tonic signaling of 41BBζ-based CARs enables normal CAR-T cell differentiation

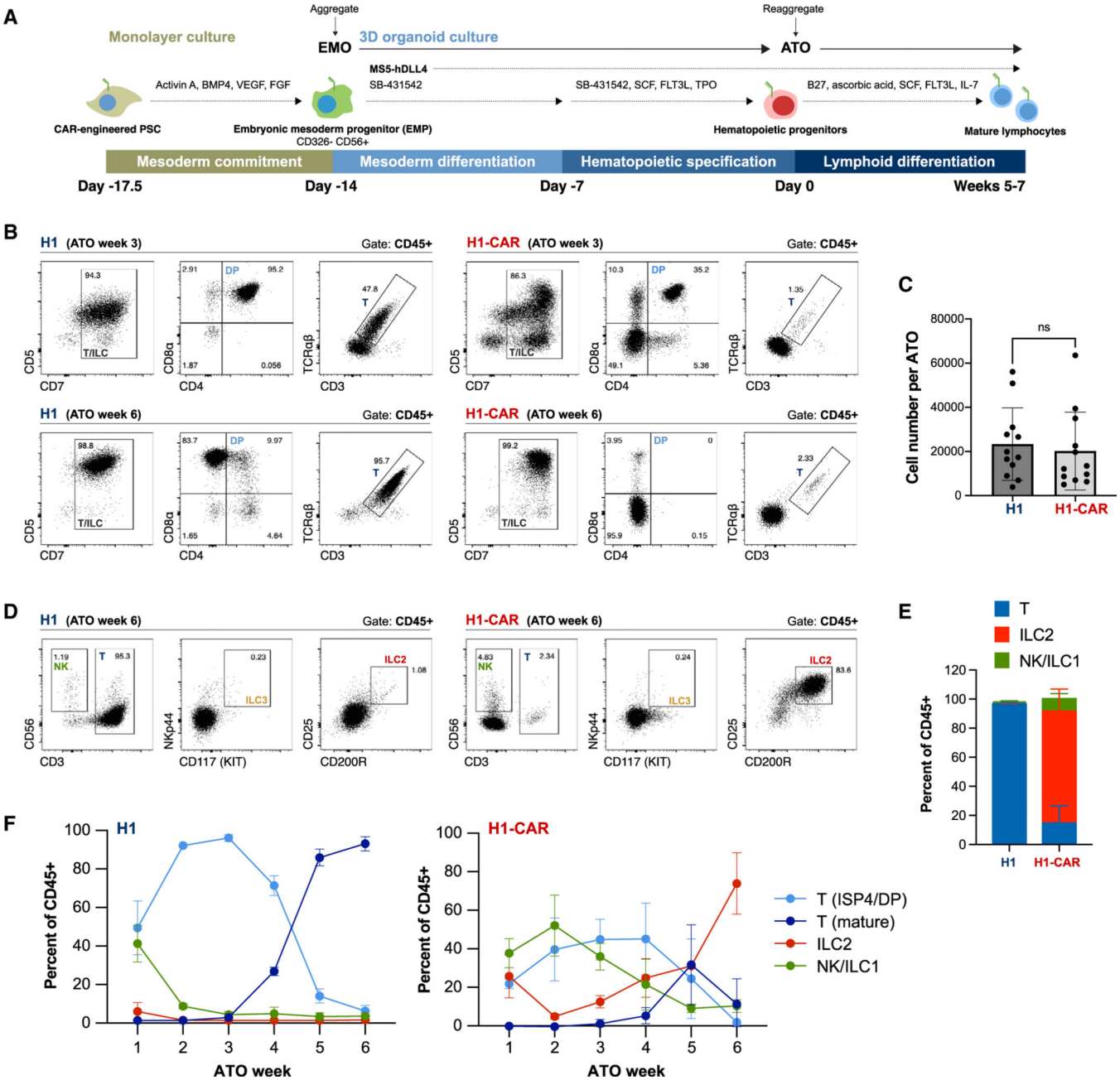

Figure 1. Constitutive CAR expression in PSCs results in impaired T cell differentiation and preferential generation of ILC2s in ATOs

(A) Schematic of the EMO/ATO differentiation protocol starting from human pluripotent stem cells (PSCs). After 3.5 days of mesoderm induction, embryonic mesoderm progenitors (EMPs) are isolated and aggregated with MS5-hDLL4 cells in embryonic mesoderm organoids (EMOs) for 2 weeks under mesoderm differentiation and hematopoietic induction conditions. EMOs are harvested, and suspension cells are reaggregated with fresh MS5-hDLL4 cells in ATOs for 5–7 weeks for lymphoid differentiation.

(B) Representative flow cytometry analysis of T cell differentiation of week 3 and week 6 ATO cultures starting from H1 and H1-CAR PSCs, gated on total CD45+ cells (n = 4).

(C) Number of total cells generated per ATO at week 6 (mean ± SD, n = 12).
(D) Representative flow cytometry analysis of NK, T cell, and ILC subsets in ATOs at week 6 starting from H1 and H1-CAR PSCs, gated on total CD45+ cells.
(E) Frequencies of T cells, ILC2s, and NK/ILC1 cells, gated on CD45+ cells (gating strategy shown in Figure S1D) (mean ± SD of technical triplicates, representative of 9 independent experiments).
(F) Frequencies of lymphoid subsets from weeks 1–6 in H1 and H1-CAR ATO cultures (gating strategy as for Figure S1D, with additional gating for mature T cells defined as CD3+ and T precursors defined as CD3−CD4+ containing DP and ISP4 precursors) (mean ± SD, n = 3).

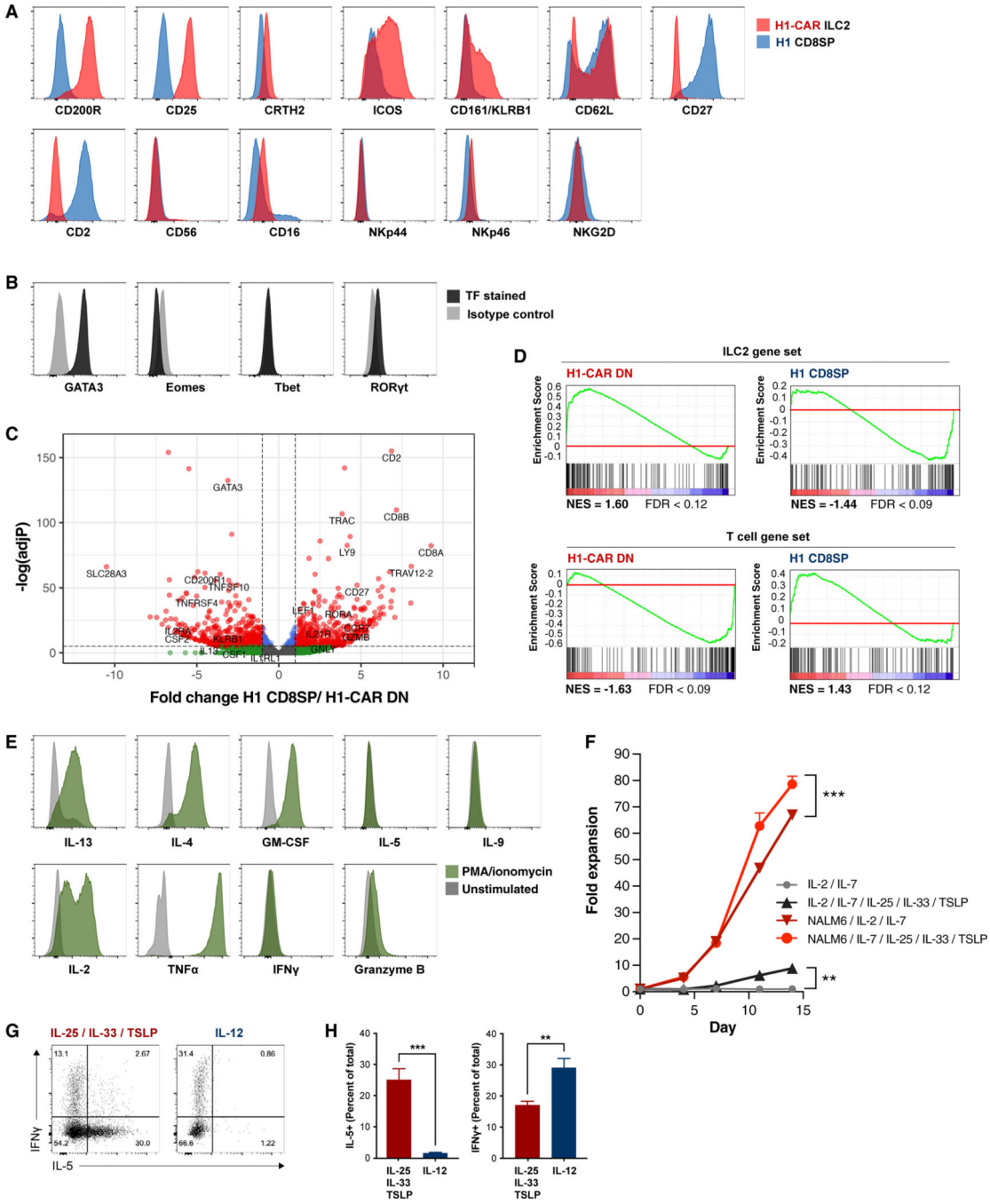

Figure 2. PSC-derived ILC2s are functional type 2 cells

(A) Flow cytometry analysis of week 7 H1-CAR ATO-derived ILC2s (red shaded) compared with CD8SP T cells generated from H1 ATO cultures (blue shaded).

(B) Representative intracellular flow cytometry analysis of transcription factor expression gated on the ILC2 population from week 7 H1-CAR ATOs (n = 2). Isotype staining controls are shown in light gray for each antibody.

(C) Comparison of gene expression by RNA-seq as fold change (FC) between H1 ATO-derived CD8SP T cells and H1-CAR ATO-derived CD8−CD4− (DN) cells enriched for the

ILC2 population. The dashed line on the y axis depicts adjusted p value of 10e–6; the dashed line on the x axis depicts log2FC > 2.

(E) Gene set enrichment analysis (GSEA) comparing H1-CAR DN and H1 CD8SP T cell differentially expressed genes ranked by log2FC with external RNA-seq gene sets from primary human fetal ILC2s and T cells (GEO: GSE163587). GSEA plots show normalized enrichment score (NES) and false discovery rate (FDR).

(E) Representative cytokine production of H1-CAR ATO-derived ILC2s after 6 h of phorbol 12-myristate 13-acetate (PMA)/ionomycin stimulation (n = 2 independent experiments).

(F) Expansion of H1-CAR ATO-derived ILC2s after serial stimulation with or without irradiated CD19+ NALM6 cells in the presence of IL-2 and IL-7 with or without IL-25, IL-33, and TSLP for 14 days. Fresh cytokines were added every 3–4 days, and irradiated NALM6 cells were added on day 0 and day 7. Fold expansion is shown (mean ± SD of technical triplicates, representative of 2 independent experiments, t test: *p < 0.5, **p < 0.01, ***p < 0.001).

(G) Representative analysis of IFNγ and IL-5 by intracellular flow cytometry of H1-CAR ATO-derived ILC2s cultured in the presence of IL-25, IL-33, TSLP, or IL-12 for 5 days, with PMA/ionomycin added for the final 6 h of culture.

(H) Frequencies of IFNγ+ and IL-5+ cells shown in (G) (mean ± SD of technical triplicates, representative of 2 independent experiments).

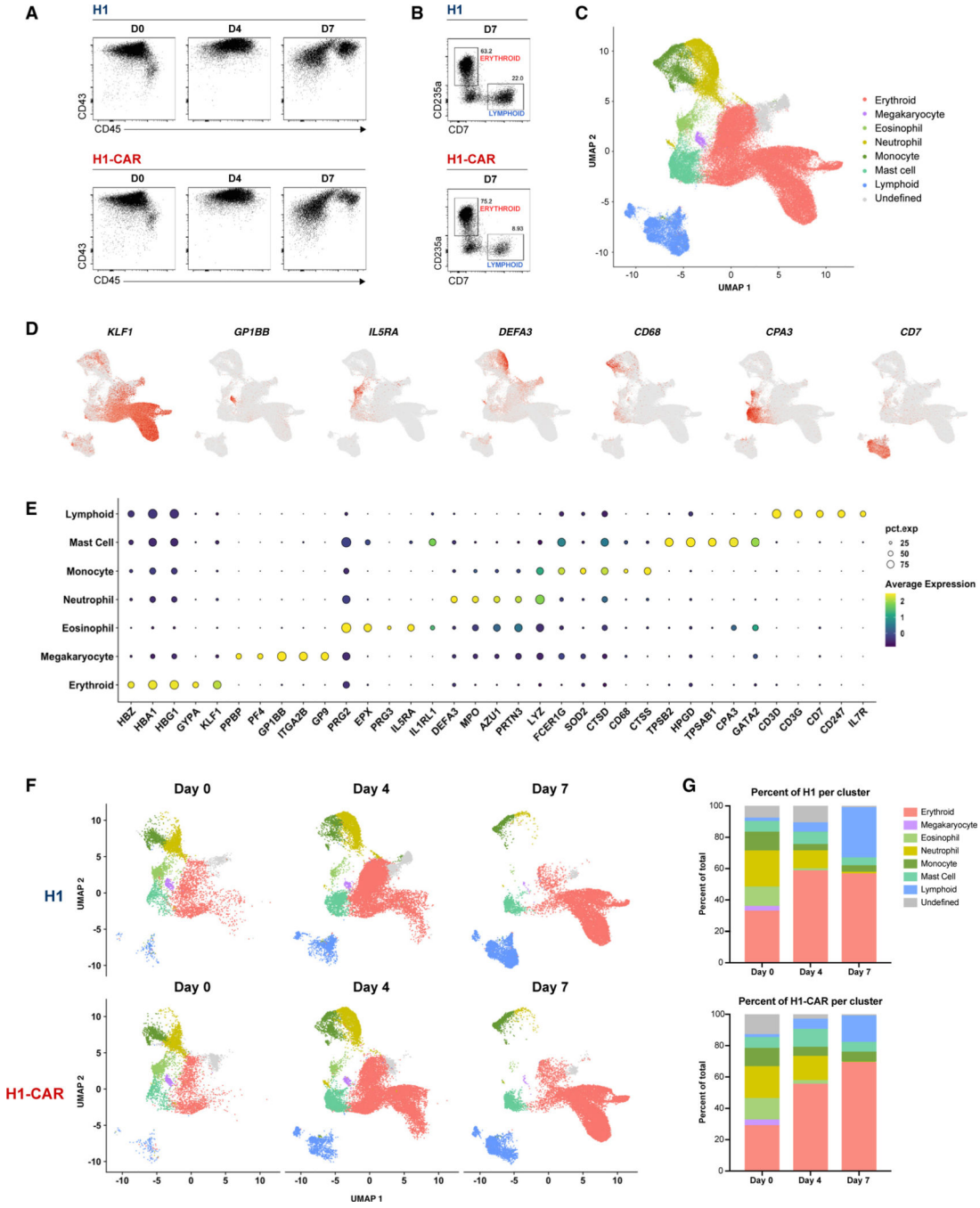

Figure 3. scRNA-seq of early PSC ATOs shows minimal effects of CAR signaling on multilineage hematopoietic development

(A) Representative flow cytometry analysis of hematopoietic differentiation based on expression of CD43 and CD45 on ATO day 0 (i.e., upon harvest from EMO cultures), ATO day 4, and ATO day 7 cultures starting from H1 or H1-CAR PSCs. Gated on total mouse CD29− (mCD29−) cells to exclude residual MS5-hDLL4 stromal cells (n = 2).

(B) Representative flow cytometry analysis of erythroid and lymphoid differentiation in day 7 ATO culture based on expression of CD235a and CD7, respectively. Gated on mCD29− cells (n = 2).

(C) UMAP projection of scRNA-seq data of sorted total DAPI− mCD29− cells isolated from H1 and H1-CAR ATO cultures on days 0, 4, and 7 (n = 2 experimental replicates per time point). All samples were concatenated for clustering. Colors represent annotated lineage clusters based on expression of lineage-defining genes.
(D) Expression of canonical genes representative of lineage clusters shown in (C).
(E) Expression of curated, lineage-defining genes for clusters shown in (C). Dot size represents the percentage of cells expressing each gene, and the heatmap shows average gene expression.
(F) UMAPs across individual ATO time points from H1 and H1-CAR ATOs. Colors correspond to the lineage clusters shown in (C).
(G) Frequencies of each cluster shown in (F) at each time point from H1 and H1-CAR ATOs.
In (A) and (B), D, day.

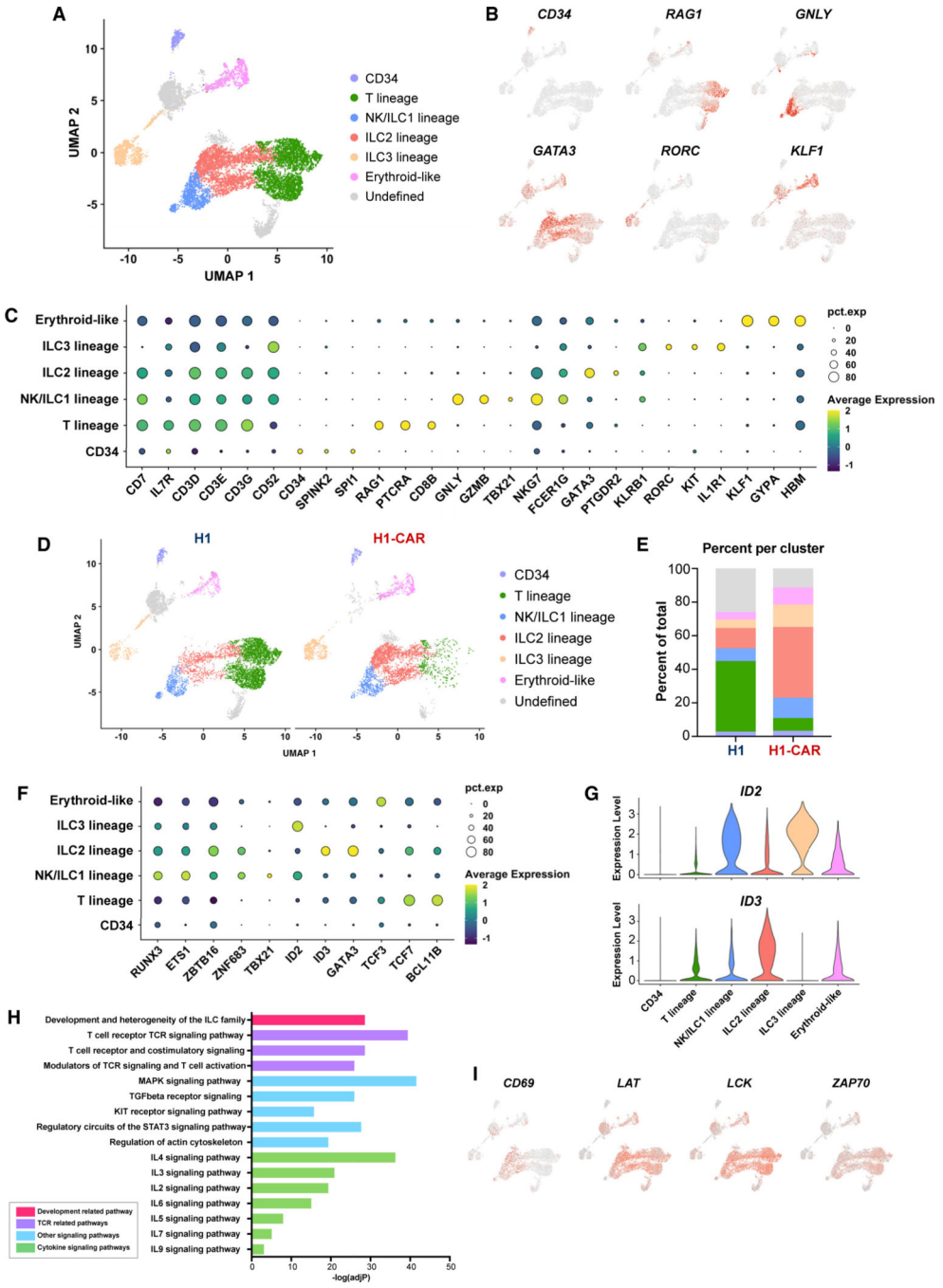

Figure 4. Lymphoid precursor cells in CAR PSC ATOs show ILC2-primed precursors enriched in TCR activation pathway genes

(A) Reclustering and UMAP of the scRNA-seq data from Figure 3C, sub-gating on the annotated lymphoid cluster. Colors represent annotated clusters based on expression of lineage-defining genes.

(B) Expression of canonical genes representative of lineage clusters shown in (A).

(C) Expression of curated general lymphoid genes and lineage-defining genes for clusters shown in (A).

(D) UMAPs showing cell clusters identified in (A) in H1 or H1-CAR ATO samples (day 0, day 4, and day 7 time points combined).
(E) Frequencies of clusters shown in (D).
(F) Expression of selected transcription factors in clusters identified in (A).
(G) Violin plots of *ID2* and *ID3* expression in clusters shown in (A).
(H) GSEA of Wikipathway gene sets in ILC2 versus T cell-lineage clusters identified in (A). Selected pathways positively enriched in the ILC2-lineage cluster are shown.
(I) Feature plots showing expression of genes encoding *CD69* and the TCR signal transduction molecules *LAT*, *LCK*, and *ZAP70* (all samples combined).

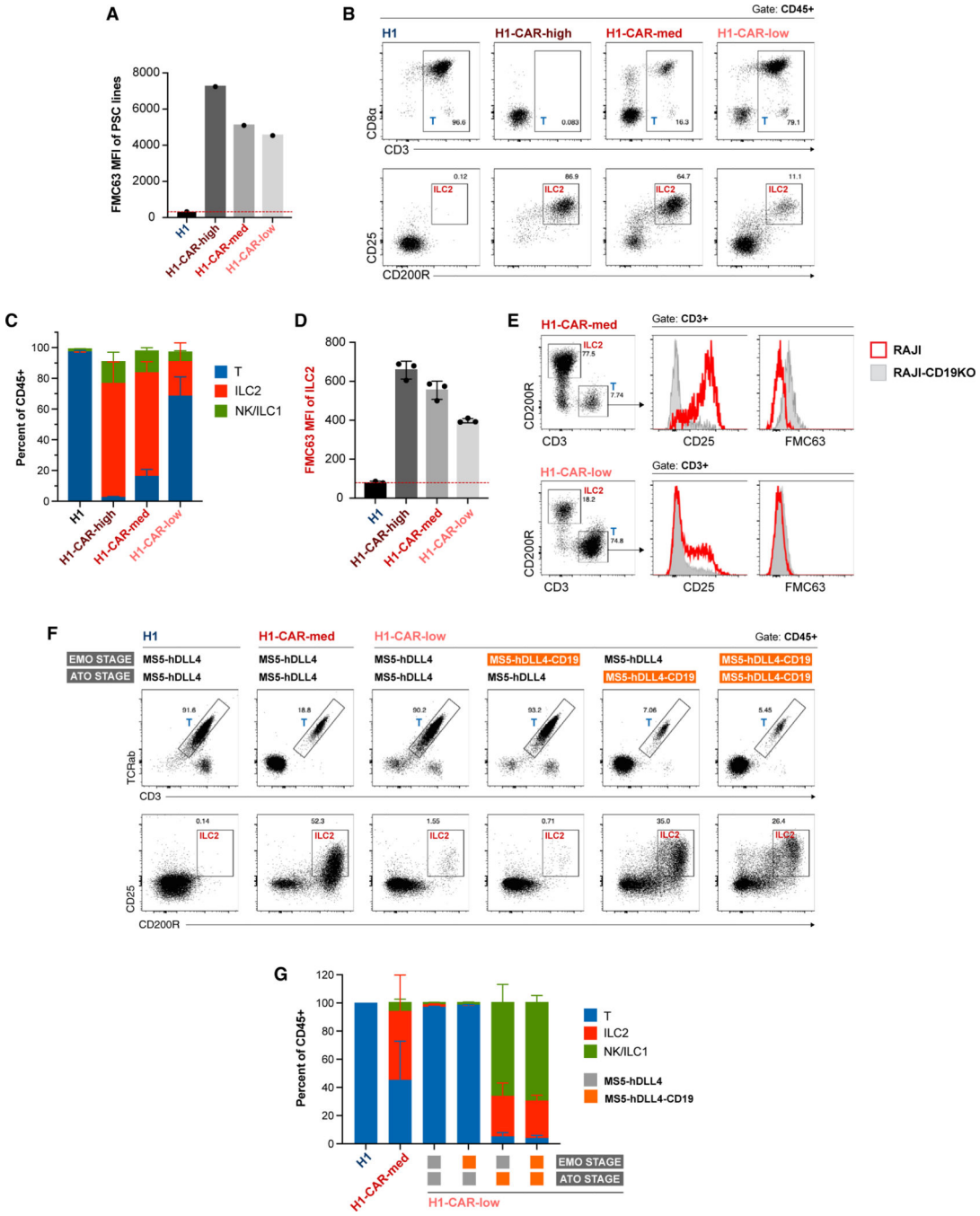

Figure 5. Tuning CAR expression level restores T cell differentiation but affects CAR activation potential

(A) Mean fluorescence intensity (MFI) of surface CAR (FMC63) staining on H1 PSC lines stably expressing the same CD19 28ζ CAR (H1-CAR.LH.28TM.28ζ) at different levels.

(B) Representative flow cytometry analysis of T cell and ILC2 differentiation in week 6 ATO cultures starting from H1 or H1-CAR PSCs with different levels of CAR expression, as shown in (A). Gated on total CD45+ cells.

(C) Frequencies of lymphocyte subsets as shown in (B), using the gating strategy shown in Figure S1D (mean ± SD of technical triplicates, representative of 3 independent experiments).

(D) MFI of surface CAR expression on ILC2s isolated from week 6 ATOs.

(E) Flow cytometry analysis of CAR-T cell activation shown by upregulation of CD25 and downregulation of surface CAR on CD3+ gated CAR-T cells. Cells were isolated from week 6 H1-CAR-med and H1-CAR-low ATOs and stimulated with CD19+ Raji (red solid line) or Raji-CD19 knockout (CD19KO) (gray shaded) cells for 24 h.

(F) Representative flow cytometry analysis of T cell and ILC differentiation in week 6 ATO cultures starting from H1-CAR-low PSCs. Normal (MS5-hDLL4) or CD19-expressing (MS5-hDLL4-CD19) stromal cell lines were used during EMO and/or ATO stages, as shown.

(G) Frequencies of lymphocyte subsets shown in (F), using the gating strategy shown in Figure S1D (mean ± SD of technical triplicates, representative of 2 independent experiments).

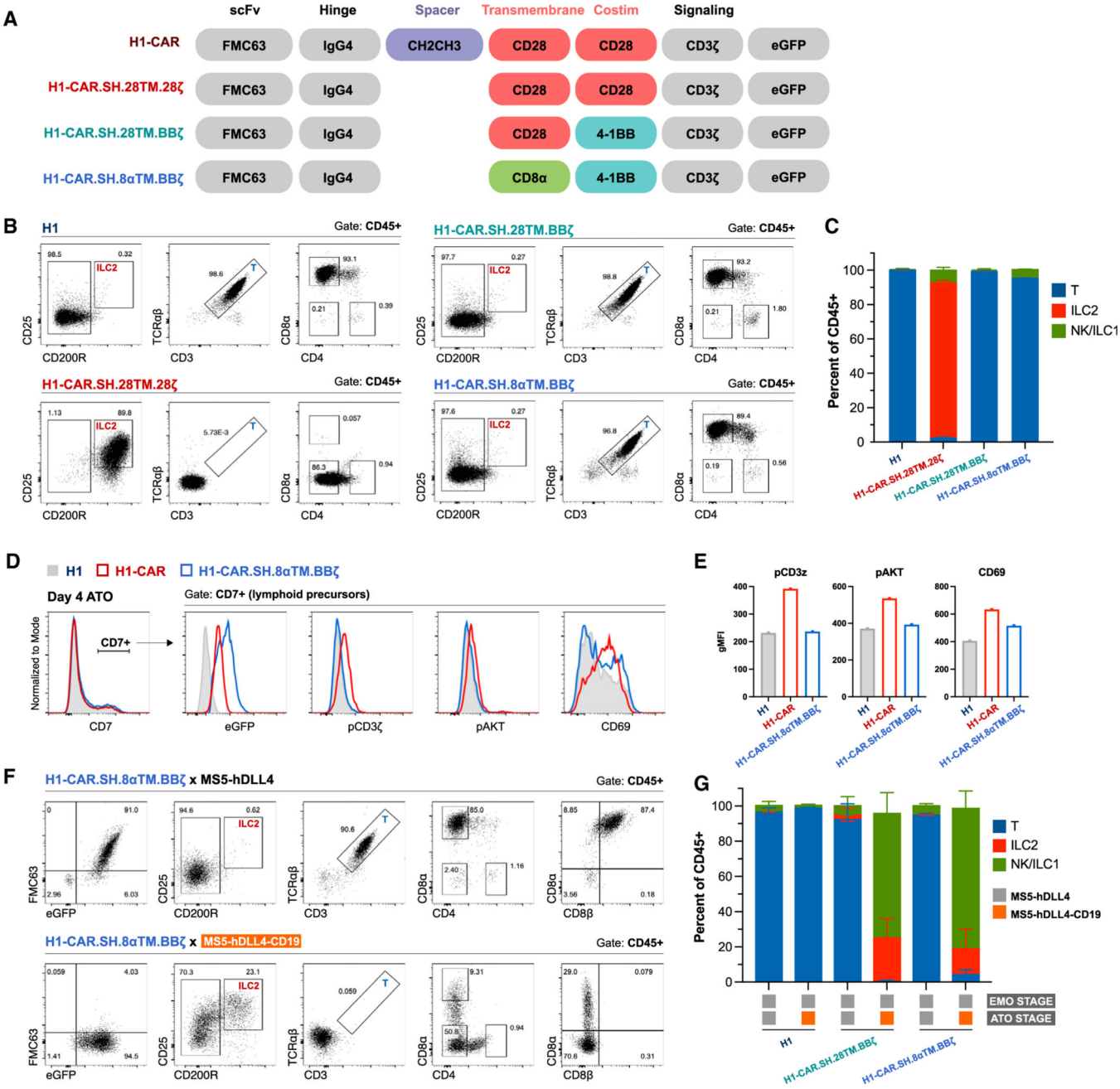

Figure 6. CAR costimulatory domain substitution permits CAR-T cell development in ATOs

(A) Schematic of the structures of CD19-targeted CARs with variations in spacer, TM, and costimulatory domains used for generation of CAR-transduced H1 PSClines. H1-CAR (H1-CAR.LH.28TM.28ζ) denotes the original CAR used in the previous experiments.

(B) Representative flow cytometry analysis of T cell and ILC differentiation in week 6 ATOs starting from H1 or H1-CAR lines expressing the alternative CARs shown in (A). Gated on total CD45+ cells.

(C) Frequencies of lymphocyte subsets of (B), using the gating strategy shown in Figure S1D (mean ± SD of technical triplicates, representative of 2 independent experiments).

(D) Representative flow cytometry analysis of CD69, EGFP (CAR marker), and phosphorylation of CD3ζ (pY142) and AKT (pS473) in CD7+ lymphoid precursors isolated from day 4 H1, H1-CAR (H1-CAR.LH.28TM.28ζ), and H1-CAR.SH.8αTM.BBζ ATO cultures.

(E) Geometric MFI of phosphorylated CD3ζ (pY142), phosphorylated AKT (pS473), and CD69 expression shown in (D) (representative of 2 independent experiments).

(F) Representative flow cytometry analysis of T cell and ILC differentiation in week 6 H1-CAR.SH.8αTM.BBζ ATOs using normal (MS5-hDLL4) or CD19-expressing (MS5-hDLL4-CD19) stromal cell lines at the ATO stage. Gated on total CD45+ cells.

(G) Frequencies of lymphocyte subsets shown in (F) (and including data for H1 control ATOs and H1-CAR.SH.28TM.BBζ ATOs), using the gating strategy shown in Figure S1D (mean ± SD of technical triplicates).

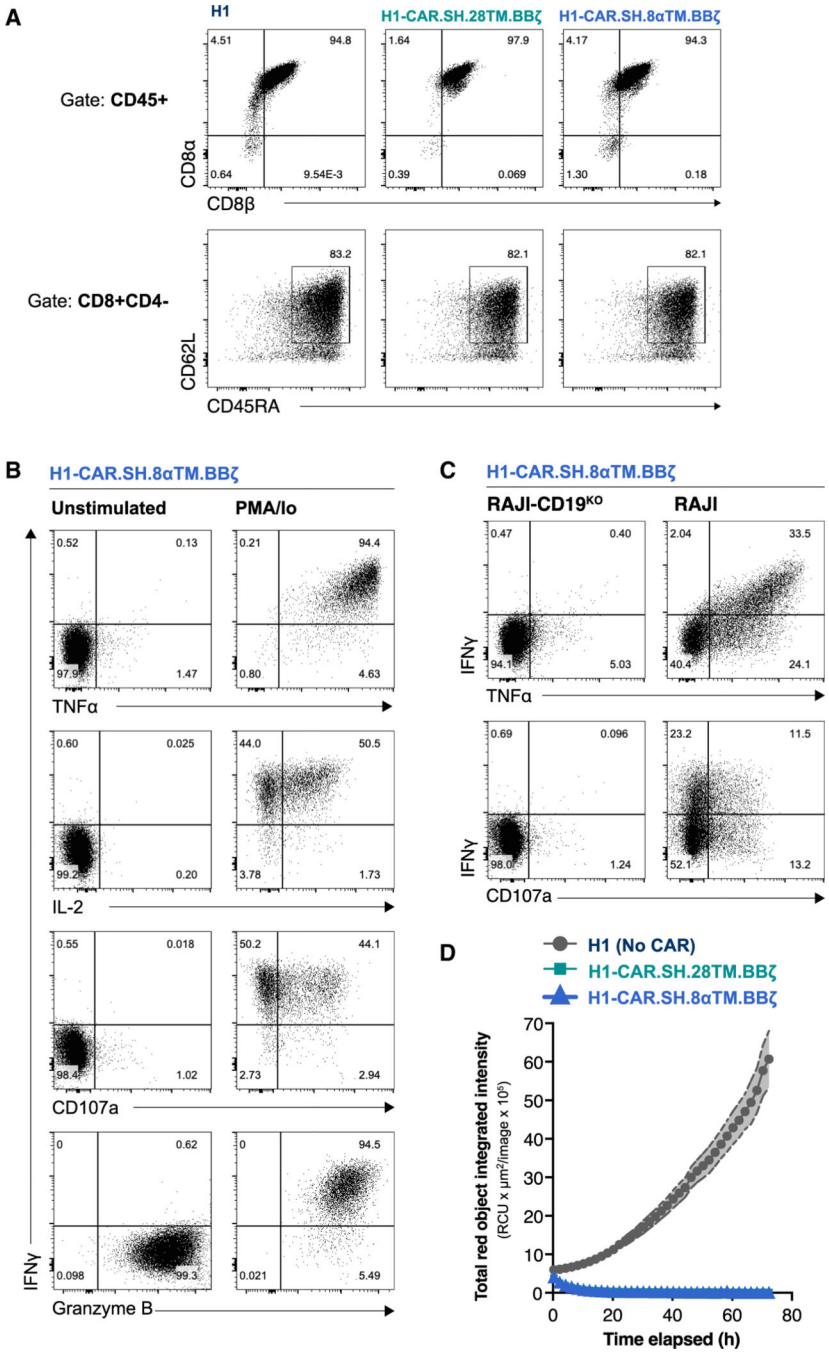

Figure 7. PSC-derived CAR-T cells with 4–1BBζ costimulatory domains are functional

(A) Representative flow cytometry analysis of T cell phenotype in H1 or H1-CAR ATOs expressing different 4–1BBζ CAR architectures shown in Figure 6C. CD8α and CD8β expression is shown gated on total CD45+, and CD62L and CD45RA expression is shown on CD8SP CAR-T cells (gated on CD45+CD3+CD8α+CD4+).

(B and C) Cytokine production and CD107a membrane mobilization of CAR-T cells isolated from H1-CAR.SH.8αTM.BBζ ATOs in response to PMA/ionomycin (B) and co-culture with Raji-CD19KO or CD19+ Raji cells (C) for 6 h.

(D)Incucyte cytotoxicity assays measuring growth of mKate+ (red fluorescent) Raji cells cocultured with T cells isolated from H1, H1-CAR.SH.28TM.BBζ, or H1-CAR.SH.8αTM.BBζ ATOs at an effector-to-target ratio of 1:1 for 72 h.

KEY RESOURCES TABLE

REAGENT or RESOURCE	SOURCE	IDENTIFIER
Antibodies		
Anti-FMC63	Acro Biosystems	Cat # FM3-BY54
Anti-human CD107a	Biolegend	Clone H4A3; RRID: AB_1279055
Anti-human CD117	Biolegend	Clone 104D2; RRID: AB_2566215
Anti-human CD127	Biolegend	Clone A019D5; RRID: AB_2563605
Anti-human CD16	Biolegend	Clone 3G8; RRID: AB_314218
Anti-human CD161	Biolegend	Clone HP-3G10; RRID: AB_11126745
Anti-human CD19	Biolegend	Clone H1B19; RRID: AB_314238
Anti-human CD2	Biolegend	Clone RPA-2.10; RRID: AB_2800717
Anti-human CD22	Biolegend	Clone HIB22; RRID: AB_2563902
Anti-human CD200R	Biolegend	Clone OX-108; RRID: AB_2565526
Anti-human CD235a	Biolegend	Clone HI264; RRID: AB_2562706
Anti-human CD25	Biolegend	Clone BC96; RRID: AB_314276
Anti-human CD294	Biolegend	Clone BM16; RRID: AB_2562468
Anti-human CD3	Biolegend	clone UCHT1; RRID: AB_2629689
Anti-human CD34	Biolegend	Clone 581; RRID: AB_1877168
Anti-human CD4	Biolegend	clone RPA-T4; RRID: AB_2564391
Anti-human CD43	Biolegend	clone CD43–10G7; RRID: AB_2563698
Anti-human CD45	Biolegend	Clone HI30; RRID: AB_2561940
Anti-human CD5	Biolegend	clone UCHT2; RRID: AB_314098
Anti-human CD56	Biolegend	Clone HCD56; RRID: AB_604107
Anti-human CD7	Biolegend	clone CD7–6B7; RRID: AB_2563941
Anti-human CD8a	Biolegend	clone SK1; RRID: AB_2565243
Anti-human CD94	Biolegend	Clone DX22; RRID: AB_2734277
Anti-human EOMES	Invitrogen	Clone WD1928; RRID: AB_2572615
Anti-human GATA3	BD Bioscience	Clone L50–823; RRID: AB_2739242
Anti-human GM-CSF	Biolegend	Clone BVD2–21C11; RRID: AB_11147946
Anti-human ICOS	Biolegend	Clone C398.4A; RRID: AB_2562545
Anti-human IFNg	Biolegend	Clone 4S.B3; RRID: AB_2563882
Anti-human IL-13	Biolegend	Clone JES10–5A2; RRID: AB_2616746
Anti-human IL-2	Biolegend	Clone MQ1–17H12; RRID: AB_2563877
Anti-human IL-4	Biolegend	Clone MP4–25D2; RRID: AB_2561679
Anti-human IL-5	Biolegend	Clone JES1–39D10; RRID: AB_315139
Anti-human NKG2D	Biolegend	Clone 1D11; RRID: AB_2728272
Anti-human NKp44	Biolegend	Clone P44–8; RRID: AB_756100
Anti-human NKp46	Biolegend	Clone 9E2; RRID: AB_2563853
Anti-human PD-1	Biolegend	Clone EH12.2H7; RRID: AB_2563212
Anti-human RORgt	Invitrogen	Clone AFKJS-9; RRID: AB_10609207
Anti-human TBET	Biolegend	Clone 4B10; RRID: AB_2561761

REAGENT or RESOURCE	SOURCE	IDENTIFIER
Anti-human TCRab	Biolegend	Clone IP26; RRID: AB_2562805
Anti-human TNFa	Biolegend	Clone MAb11; RRID: AB_10960738
Anti-mouse CD29	Biolegend	Clone HMb1–1; RRID: AB_528790
Anti-CD247 (pY142)	BD Biosciences	Clone K25–407.69; RRID: AB_647237
Anti-Akt (pS473)	BD Biosciences	Clone M89–61; RRID: AB_2737674
Anti-Biotin	Biolegend	Clone 1D4-C5; RRID: AB_10641847
Bacterial and virus strains		
pCCL-c-UBC-aFMC63-IgG4-CH2CH3-28TM-28–3z (lentivirus)	This paper	N/A
pCCL-c-UBC-aFMC63-IgG4–28TM-28–3z (lentivirus)	This paper	N/A
pCCL-c-UBC-aFMC63-IgG4(short)-28TM-BB-3z (lentivirus)	This paper	N/A
Chemicals, peptides, and recombinant proteins		
rhActivin A	R&D Systems	Cat. 338-AC-010
rhBMP4	R&D Systems	Cat. 314-BP-010
rhVEGF	R&D Systems	Cat. 298-VS-005
rhFGF	R&D Systems	Cat. 233-FB-025
ROCK inhibitor Y-27632 dihydrochloride	Tocris Bioscience	Cat. 1254
TGF-bRI inhibitor SB-431542	Tocris Bioscience	Cat. 1614
rhIL-7	R&D Systems	Cat. 207-IL-025
rhSCF	R&D Systems	Cat. 255-SC-050
rhFLT3L	R&D Systems	Cat. 308-FK-025
rhTPO	R&D Systems	Cat. 288-TP-025
rhIL-2	Peprotech	Cat. 200–02
rhIL-12	Peprotech	Cat. 200–12
rhIL-25	Peprotech	Cat. 200–24
rhIL-33	Peprotech	Cat. 200–33
rhTSLP	Peprotech	Cat. 300–62
B27 supplement (50X)	GIBCO	Cat. 17504–044
Accutase	Innovative Cell Technologies	Cat. AT-104
TrypLE Express	GIBCO Life technologies	Cat. 12604–013
Annexin V	Biolegend	AB_2616657
TruStain FcX	Biolegend	Cat. 422302
DAPI	Life technologies	Cat. D1306
Matrigel® Growth Factor Reduced (GFR) Basement Membrane Matrix, Phenol Red-free, LDEV-free,	Corning	Cat. 356231
mTeSR Plus	Stem Cell Technologies	Cat. 100–0276
X-VIVO 15 Serum-free Hematopoietic Cell Medium	Lonza	Cat. 04–418q
EGM-2, Endothelial Cell Growth Medium-2 Bullet Kit	Lonza	Cat. CC-3162
RPMI 1640	Corning	Cat. 10–040-CV

REAGENT or RESOURCE	SOURCE	IDENTIFIER
GLutaMAX Supplement	ThermoFisher Scientific	Cat. 35050061
L-Ascorbic acid 2-phosphate sesquimagnesium salt hydrate	Sigma	Cat. A8960
Penicillin-Streptomycin (100X)	GeminiBio	Cat. 400–109
Critical commercial assays		
Cell Stimulation Cocktail (plus protein transport inhibitors)	eBioscience	Cat. 00–4975-03
Intracellular Fixation & Permeabilization Buffer Set	eBioscience	Cat. 88–8824-00
True-Nuclear™ Transcription Factor Buffer Set	Biolegend	Cat. 424401
Zombie Aqua™ Fixable Viability Kit	Biolegend	Cat. 423102
CD326 (EpCAM) MicroBeads, human	Miltenyi	Cat. 130–061-101
Dead Cell Removal Kit	Miltenyi	Cat.130–090-101
Anti-PE MicroBeads	Miltenyi	Cat. 130–048-801
RNeasy Micro kit	QIAGEN	Cat. 74004
Deposited data		
Bulk RNAseq data of H1 derived CD8 T cells	Montel-Hagen et.al, 2019[9]	GEO: GSE116015
Bulk RNAseq data of H1-CAR derived DN cells	This paper	GEO: GSE216251
Single cell RNAseq data of H1 and H1-CAR derived precursor cells	This paper	GEO: GSE224964
Experimental models: Cell lines		
H1 ESC line	WiCell	https://www.wicell.org/
ESI-017 ESC line	ESI BIO	https://www.esibio.com/media/wysiwyg/esibio/documents/esicells/WEB_Rev_B_ESI-017_Data_Sheet.pdf
N11 T-iPSC line	Cedars-Sinai iPSC Core and Cedars-Sinai Biomanufacturing Center, Los Angeles, CA	N/A
MS5-hDLL4	Montel-Hagen et al., 2019[9]	N/A
MS5-hDLL4-CD19	This paper	N/A
MS5-hDLL4- A2/MART1	This paper	N/A
MS5-hDLL4- A2/ESO	This paper	N/A
H1-CAR-high	This paper	N/A
H1-CAR-med	This paper	N/A
H1-CAR-low	This paper	N/A
H1-CAR-28TM-28–3z	This paper	N/A
H1-CAR-28TM-BB-3z	This paper	N/A
RAJI-eGFP	Yvonne Chen, UCLA	N/A
RAJI-eGFP-CD19KO	Yvonne Chen, UCLA	N/A
Recombinant DNA		

REAGENT or RESOURCE	SOURCE	IDENTIFIER
pCCL-c-UBC-aFMC63-IgG4-CH2CH3–28TM-28–3z (lentivirus)	This paper	N/A
pCCL-c-UBC-aFMC63-IgG4–28TM-28–3z (lentivirus)	This paper	N/A
pCCL-c-UBC-aFMC63-IgG4(short)-28TM-BB-3z (lentivirus)	This paper	N/A
Software and algorithms		
FlowJo	Tree Star Inc.	https://www.flowjo.com/solutions/flowjo
GraphPad Prism	GraphPad Software	https://www.graphpad.com/scientificsoftware/prism/
Seurat	Hao et al., 2021[76]	https://satijalab.org/seurat/index.html
EnhancedVolcano	Blighe et al., 2018[77]	https://www.bioconductor.org/packages/release/bioc/vignettes/EnhancedVolcano/inst/doc/EnhancedVolcano.html
GSEA	Subramanian et al., 2005[37]	https://www.gsea-msigdb.org/gsea/index.jsp